The centennial sustainable assessment of regional construction industry under the multidisciplinary coupling model

Zhiwu Zhou[a,*], Ji Zhou[a], Bo Zhang[a] , Julián Alcalá[b] , Víctor Yepes[b]

[a] *Hunan Engineering Research Center, Hunan University of Science and Engineering, Yongzhou Hunan, People's Republic of China*
[b] *Institute of Concrete Science and Technology (ICITECH), Universitat Politècnica de València, València, Spain*

ABSTRACT

Sustainability research in the construction industry is of great strategic significance to the ecological environment of countries worldwide. This paper innovates theoretical models such as "structural response sensitivity weight" through interdisciplinary research on advanced mathematics, engineering science, computer science, environmental management and economic sociology. The model solves the limitations of multi-factor, multi-discrete, multi-constraint and low coupling iteration accuracy. The article shows the robustness of the model through case studies. The research data shows that the construction industry in China will reach its highest life cycle assessment emission peak of 2.73 GT in 2030 and will have harmful emissions of -2.78 GT between 2061 and 2098. The social impact assessment will peak at 4.26 GT in 2048 and harmful emissions of -3.75 GT per year from 2061 to 2098. This research provides a comprehensive research theory system and reference standards for scientific calculation and accurate assessment of the sustainable development of the construction industry in various countries around the world.

Keywords: Gross domestic product; Life cycle cost; Life cycle assessment; Social impact assessment; Topology optimization

1. Introduction

The United Nations Framework Convention on Climate Change COP24" held in Poland on Dec. 5, 2018, announced a 2.5% increase in global carbon emissions from developed countries and emerging economies, the world is predicted to reach a temperature increase of 1.5℃ between 2030 and 2053 due to global warming, with a continued warming rate of 0.2℃ per decade (Deraemaeker and Worden, 2018). Central international policies on climate change – Paris Agreement (UNFCCC, 2015), 2030 Agenda for Sustainable Development (United Nations, 2015), New Urban Agenda (United Nations, 2017), sustainable development of urban areas be explicitly seen as an enabler and core target of climate change. Climate change remains a pressing challenge for all nations (Ebhota and Tabakov, 2021).

1.1. Main Regional and National Sustainable Goals and Current Situation of the Construction Industry

The author searched articles (2000-2023) published in three primary databases (Web of Science, Google Scholar and Scopus) according to the title 1.1, resulting in a total of 6340 articles. The long-term planning goals for 2050-2060 in 10 countries and regions (accounting for 96% of total global carbon emissions) and the current status of carbon emissions in the construction industry in each country were checked based on the content of directly related articles. Unfortunately, no published research results have been found that can prove the scientific nature and effectiveness of each country's planning goals (Table 1, marked as NO).

Table 1

The status of sustainable development and ecological environment impact in the global construction industry.

Region	Strategy	Status	Long-term goal	References	Result
Global	The Paris Agreement	The construction industry will account for over 31% of total carbon emissions in 2020 and 52% by 2050.	Achieving global net-zero emissions around the midcentury, which is required to cap global warming at 1.5 C above preindustrial levels as called for in the 2015 Paris Agreement.	(Venturini et al., 2023; Tranter et al., 2023)	NO
European Union	Long-Term Low Greenhouse Gas Emission Development Strategy of the European Union and its Member	The construction industry accounts for over 40% of the total energy consumption.	Achieving the goal of climate neutrality by 2050.	(Casals, 2006; Ozarisoy & Altan, 2022)	NO
China	Mid-Century Strategy for Deep Decarbonization	In 2019, the construction industry emitted 2.1 billion tons, accounting for 21% of the total carbon emissions.	China promised at the 75th United Nations (UN) General Assembly in 2020 to reach its carbon peak by 2030 and carbon neutrality by 2060.	(Zhou et al., 2023; Jiang et al., 2022)	NO

United States	Mid-Century Strategy for Deep Decarbonization	Construction activities are responsible for 40% of carbon emissions of non-transportation mobile sources.	At least 80% reduction of GHG emissions by 2050 compared to 2005.	(Shi et al., 2023; Liu & Xin, 2023)	NO
United Kingdom	The Clean Growth Strategy	Construction related activities account for 47% of the total carbon dioxide emissions.	Reduction of GHG emissions by 80% compared to 1990 by 2050.	(Lu et al., 2016; Eze et al., 2022)	NO
South Korea	South Korea's Carbon Neutrality Strategy for A Sustainable and Green Society in 2050	The carbon emissions of the construction industry account for 23% of the total national carbon emissions.	Achieving carbon neutrality by 2050.	(Beaudoin et al., 2023; Zhao, 2023)	NO
Australia	Long-Term Strategy 2050	Approximately 23% of total greenhouse gas emissions are the result of energy demand in the construction industry.	Achieving climate neutrality by 2050.	(Ropo et al., 2023; Pan et al., 2023)	NO
Germany	Climate Action Plan 2050	The construction industry in Germany emits 5.6671 million tons, accounting for 1.1% of the global emissions.	55% reduction of GHG emissions by 2030, 70% by 2040 and 80%–90% by 2050 compared to 1990, guided by the general goal of global greenhouse gas neutrality by 2050.	(Yu et al., 2023; Swanson, 2023)	NO
France	National Low-carbon Strategy	The construction industry in France accounts for 30% of the country's emissions.	Achieving the carbon neutrality goal by 2050.	(Li et al., 2021; Pellan et al., 2022)	NO
Japan	The Long-Term Strategy under the Paris Agreement	The emissions from Japan's construction industry reached 175.29 million tons, accounting for 3.4% of the total.	Proclamation of a "decarbonized society" as its ultimate goal, and reduction of GHG emissions by 80% by 2050 compared to 2013.	(Du et al., 2018; Onat & Kucukvar, 2020)	NO
Switzerland	Switzerland's Long-Term Climate Strategy	The total carbon dioxide emissions in 2015 were 37.28 million tons, of which 30% were caused by building materials.	Achieving net-zero GHG emissions by 2050.	(CHAI, 2022; Wiprächtiger et al., 2023)	NO

1.2. Sustainability in the construction industry and urban climate change

The ecological sustainability of the construction industry involves conducting construction activities in a manner that considers the industry's impact on society, the environment, and the economy from the cradle to the grave (Aghimien et al., 2019). To reduce building materials while maintaining safety, quality, and durability standards, researchers have proposed structural optimization methods focusing on size optimization, shape optimization, and topology optimization (Meng et al., 2020). The conceptual design stage aims to find the optimal structural design by minimizing unnecessary materials. Commonly used research methods include the level set method, homogenization, compensation method, and equivalent topology (L. Zhou et al., 2019). However, despite decades of structural optimization research, much of the focus has been on optimizing small components and individual parts, with limited systematic research and practical comparative design of large-scale indeterminate structures (Li et al., 2020). This article aims to fill the gap in this field by conducting 3D coupled optimization research on hyperstatic structures.

The optimized design of urban buildings is a tool for mitigating climate change. The aim is to identify goals, strategies and principles for sustainable building design from a macro perspective. In contrast, at the micro level, design patterns contribute to reducing CO2 emissions, ultimately reducing the vulnerability index of the urban construction industry system (Beaudoin et al., 2023). such as the American Association of State Highway and Transportation Officials (AASHTO) LRFD Bridge Design Code (AASHTO 2012), European Committee for Standardization (CEN) 1990, 1991 and 1992-2 (EN1990), British Standards Institution (BSI) 2214 Building Code (BSI, 2010), Joint Committee on Structural Safety (JCSS), International Bridge and Institute of Structural Engineering (IABSE) Approved Eurocode. Chinese Codes JTG D60-2015 and JTG/T 3365-01-2020 (Enright et al., 2013) are based on the probabilistic limit state design concept. Design codes in each country consider the unique characteristics of bridges in the region. Assessing the robustness and redundancy of bridge structures through a quantitative and scientific method is a common practice worldwide (Navarro et al., 2018).

1.3. Innovation and research objectives of this article

This article proposes a new research approach to optimize and assess the global construction industry by examining bridges' robust coupling optimization design in representative economic regions within a country. Using high-dimensional interpolation fitting approximation calculation, the optimal impact curve of the sustainable impact of the bridge construction industry in each region is determined. Through Andrews's multivariate data matrix analysis, the best sustainable impact curve for the entire country's construction industry is obtained (Landler et al., 2022). The analysis is based on the obtained national sustainable impact curve, national investment in the construction industry LCC data, and national GDP data, using a scientifically compiled algorithm model program. The article uses this analysis to predict the future sustainable impact of the country's construction industry (Fig. 1).

This research adopts a multidisciplinary approach, combining expertise from advanced mathematics, engineering, computer science, environmental management, and economic sociology. The theoretical framework incorporates green innovation, multi-dimensional green supply chain management (GSCM), and computer-integrated design (Hu et al., 2020). The research employs super-large bridges in the construction industry's four most economically advanced regions (Hubei Province, Jiangsu Province, Henan Province, and Guangdong Province) as exemplars for three-dimensional analysis to enhance its robustness and minimize uncertainty. Regression analysis and scientific algorithms formulate the optimal regional and national sustainable impact optimization equation. The article calculates and evaluates the sustainable impact on the country's future construction industry through a scientifically derived curve model. The validity and practicality of the theoretical framework are established through case analysis. This research provides a helpful optimization standard for construction and structural designers.

The article is structured into five sections: In the first section, an introduction, the global sustainability status, and the impact of the construction industry on a global scale are discussed. The second section, methodology, outlines the scientific algorithm model's research theory and procedures. The third section, results, presents the case of finite element analysis and structural topology optimization (TO). The fourth section, the discussion, analyzes the impact of the construction industry case on global sustainability. The final section, conclusions, summarizes the research findings, highlights the significance of the research, and identifies the direction for future research in this field.

2. Methodology

The primary purpose of this section is to establish multiple theoretical models and research framework systems for the entire article and establish norms and standards for case studies (Figs. 1, 3).

The research model is based on performing a three-dimensional solid finite element analysis on the bridge structure to identify any redundant components (Cooper et al., 2020). The objective of the topology optimization is to optimize the utilization of materials in the bridge members, which results in the determination of the best structural system. The analysis considers the assessment and influence curve models of regional (Specifically referring to four provinces) economic indicators derived from fitting analysis (Z.W.Zhou et al., 2022a). China's GDP data from 2021 to 2100 was analyzed. China's GDP sustainable impact curve model is based on the GDP data released by the Chinese government (2008-2020) and existing published articles (Section 4.2). China's GDP data from 2021 to 2100 is analyzed through algorithmic procedures and the generated impact curve model.

The research starts with selected cases and gradually expands from point to surface. The research route is bridge sustainability, regional and national construction industry sustainability, and sustainable analysis of the construction industry in the next 100 years (Fig. 1). This research aims to research the sustainable impact of China's construction industry on global ecology within 100 years. It only regards wind load as static gust load and excludes the impact of accidents and earthquakes. These design codes state that multiple random and seismic actions cannot be used simultaneously in combined loading (Di Cesare et al., 2021). After the bridge structure is TO, the original design structure must not be damaged.

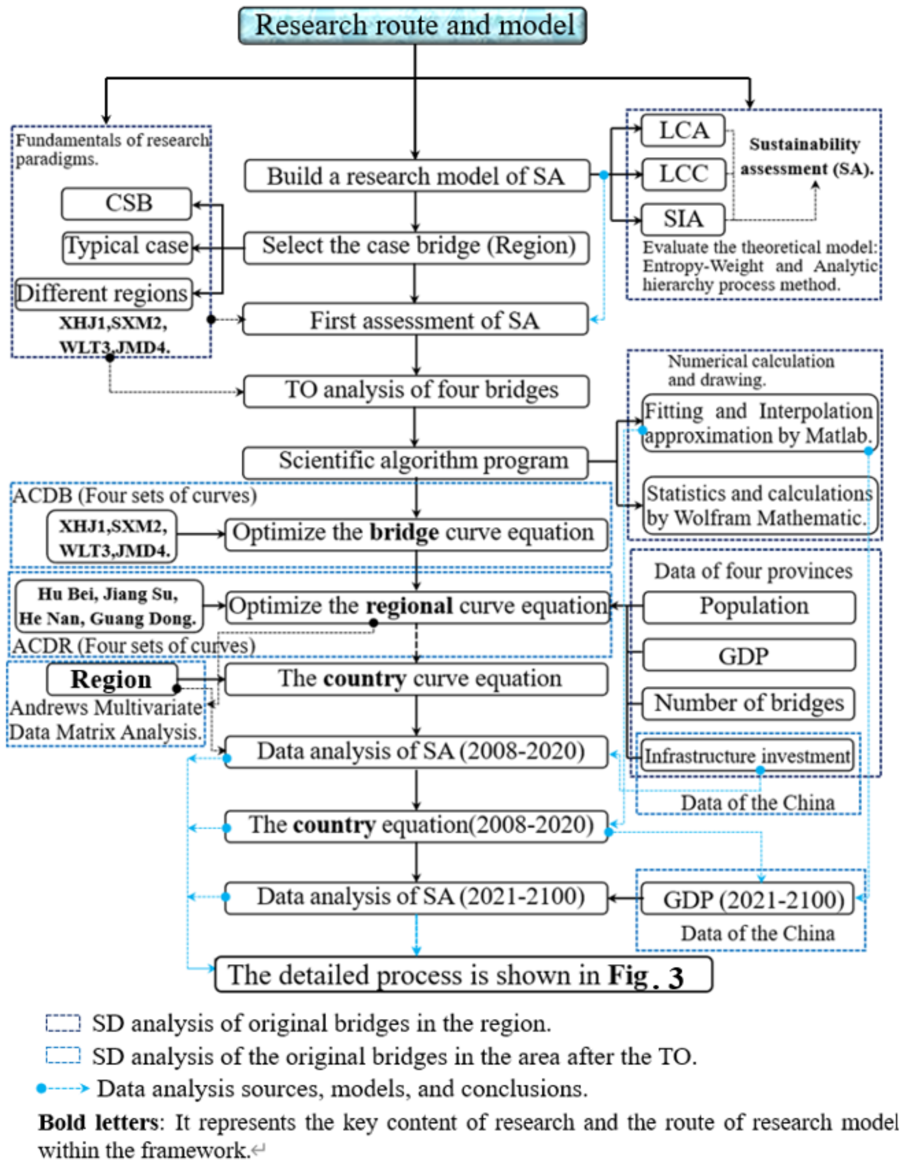

Notes: CSB = Cable stayed bridge; SA = Sustainability assessment; FEA = Finite element analysis; RE = Regional Equation (Eq); RC = Reinforced concrete; ACDB = Analysed the comprehensive data in the bridges (four sets of curves); ACDR = Analysed the comprehensive data in the regional (four sets of curves).

Fig.1 provides a detailed description: 1. The article completes the coupling optimization analysis of four cable-stayed bridges selected from four provinces. 2. Use OpenLCA software and economic analysis to obtain the four bridges' LCA, SIA and LCC data. After importing the data according to the compiled computer algorithm program, the sustainable development impact curves of the four provinces were obtained. 3. Obtain the impact curve through the GDP data of the four provinces released by China (2008-2020) and two analyses. Use the algorithm program to analyze the LCA and SIA data of the four provinces (2008-2020). 4. Conduct Andrews multivariable matrix analysis on the LCC, LCA and SIA data from the four provinces and select the optimal assessment model combination: $LCA_{\text{Guang Dong}} \rightarrow LCC_{\text{Jiang Su}} \rightarrow SIA_{\text{Jiang Su}}$. 5. Establish an impact curve for the sustainable development of China's construction industry based on the obtained $LCA_{\text{Guang Dong}} \rightarrow LCC_{\text{Jiang Su}} \rightarrow SIA_{\text{Jiang Su}}$. 6. Analyze China's GDP data from 2021 to 2100 through Chinese government announcements and related published articles. 7. Based on the data obtained in 6, the influence curve established in 5, and the algorithm program analysis, the LCA and SIA data for 2021-2100 are obtained.

Fig. 1. Description of the research route and model.

The topology optimization method involves reinforcing concrete (RC). The commonly used elastic-plastic continuous medium damage theoretical model is employed in finite element analysis of large structures made of RC materials (Penadés-Plà et., 2019). However, the application of the topology optimization method proposed by Bends Øe and Kikuchi (1988) in the construction industry presents a challenge: accurately combining numerical optimization tools with the constitutive model (Huang and Eckelman, 2022). This article addresses this challenge by utilizing effective theoretical models, analysis procedures, and models to achieve a successful outcome.

2.1. Microstructure models of topology optimization

After the completion of topology optimization (TO) on the bridge structure, individual lattices can be extracted for energy analysis to observe stress changes in internal components (Figs. 2a, 2b). The elements were divided into groups numbered 1, 2, and 3. Groups 1 and 2 represent the internal energy of the structure after TO, with a symmetrical distribution of internal forces, effective stress, and energy (Figs. 2b1, 2b2). The entire element exhibits a center-symmetric structure. Upon completion of TO on monomer three, the system was damaged, reformed, and balanced. Four slices, 3-1, 3-2, 3-3, and 3-4, were extracted and analyzed, revealing asymmetric diffusion of internal forces and an irregular, discrete structure (as compared to groups 1 and 2). The analysis of these slices revealed that some internal micro monomers were destroyed and reorganized after the TO structure, leading to a reduction in size in the low-stress region and irregular distribution of internal energy (Cai et al., 2020). This highlights the internal mechanism and microscopic nature of finite element coupled topology optimization.

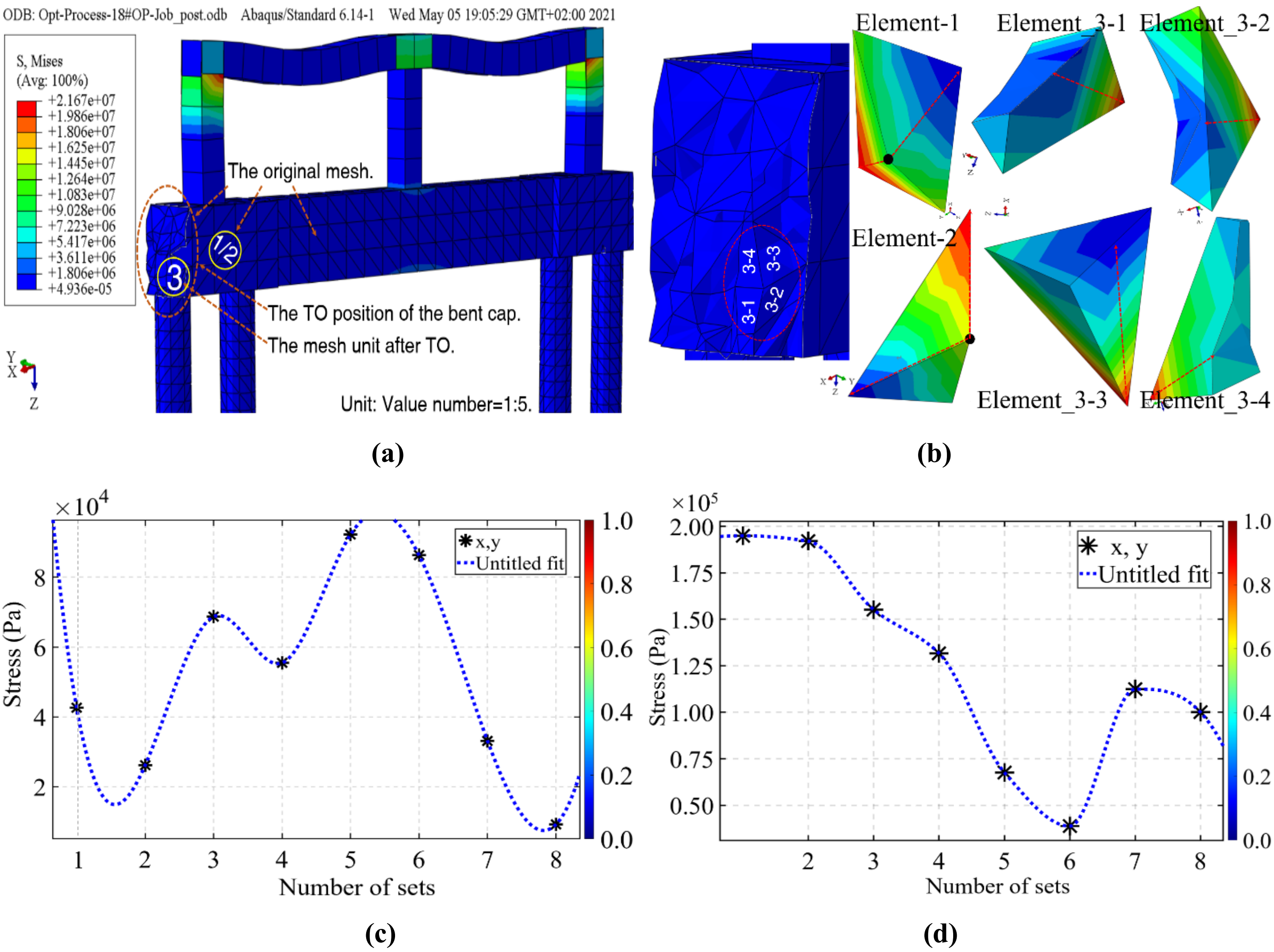

Fig. 2. Analysis of structural set and set internal force analysis after TO, a-d: (a) Component TO internal. (b) Every set. (c) V decreased. (d) V unchanged.

Linear interpolation analysis was conducted on the micro-element analysis data, resulting in a highly accurate fit with a residual sum of squares (SSE) value of 0. Spline interpolation analysis was performed on 3-1, 3-2, 3-3, and 3-4 (shown in Fig. 2c), which showed an irregular stress fluctuation but a constant internal energy dispersion and stability within the structure after five iterations and balancing. For 1 and 2, chip interpolation analysis was performed (shown in Fig. 2d), which showed a decrease in stress and internal energy in the early stage. After two-thirds of the internal energy transfer in the structure, the overall mis distributed stress was redistributed to achieve complete local stress stability.

Nodes are considered as design variables to estimate the material density field. The primary function of the Lagrange finite element is to continuously evaluate the interpolated density field to attain a smooth approximation of the material distribution (Rahmatalla and Swan, 2004). These findings indicate that the TO model's density field interpolation is an appropriate optimization technique.

2.2. Model of SRSW and SA

As analyzed in the preceding section, the core of the material TO model is to compress the volume while adhering to minimum design criteria and eliminating unnecessary physical components to attain structural optimization (Carbonell et al., 2011). The node variable is expressed as follows:

$$\begin{cases} \text{Minimize } C = \sum_{e=1}^{N_e} u_e^T K_e S_e D_e \\ 0 < \rho_i \leq \rho(x) < 1 \\ i = 1, 2, \cdots, N \end{cases} \tag{1}$$

C is set minimum volume; u_e^T is total displacement matrix of finite elements from e to N_e; K_e is the global-level stiffness matrix of the element; S_e is node elastic matrix; D_e is node deformation matrix; ρ_i is i node minimum density.

Sensitivity analysis: the derivative of the design variable of the objective function in Eq (1) is:

$$\frac{\partial V}{\partial \rho_i}'' = \int_{\Omega}^{0} \hat{\varphi}_i(x)\, d\Omega \tag{2}$$

Eqs (1) and (2) are the standard analysis models used to find the iterative methods for minimizing discrete variables and linear finite element homogeneous materials (Forman et al., 2020). This research developed a model, the "Structural Response Sensitivity Weight (SRSW)," to determine more accurately and intuitively the TO results.

In the TO analysis model established in the Methodology section, four variables, namely monitoring data, strain, stress, displacement, and energy, are the key factors affecting the structural dynamic response and optimization design. The innovative "SRSW" model replaces the theoretical model in the Methodology section to enhance the iterative convergence under the impact of multiple factors, which can more precisely evaluate the dispersion and robustness of the influencing factors.

$$Q_c(e,d) = \frac{e_m - \overline{e_g}}{d_m - \overline{d_g}} \tag{3}$$

Q_c is the sensitivity weight of structural response; d_m is maximum displacement value of each observation point (m); $\overline{d_g}$ is average displacement of all observation points at the structure where the observation points are located (m); e_m is the maximum energy value of each observation point (J); $\overline{e_g}$ is average energy of all observation points at the structure where the observation points are located (J).

The principles outlined in the Ri Declaration on sustainability assessment for sustainable development emphasize the importance of considering the interplay between the three pillars of the environment, economy, and society (Molina-Moreno et al., 2017). ISO14040 (2006) defines LCA as a systematic evaluation of a product or system's environmental inputs, outputs, and impacts over its life cycle (Salas and Yepes, 2018). Zhou et al. (Z.W. Zhou et al., 2020) conducted a comprehensive study on the five-stage sustainability assessment for bridges and developed a complete assessment framework and model. This research framework serves as a critical reference in this article, and both are crucial to understanding the sustainable impact of the construction industry in a specific region.

The focus of the research was primarily on the design, material selection, and construction phases, with little consideration given to the maintenance and recycling phases, which have a lesser impact on the environment.

The research utilized OpenLCA 1.10.1 as its LCA analysis software. It relied on Ecoinvent, Mat Web, Bedec, PSILCA, and SHDB and design drawing data for its database (Z.W. Zhou et al. 2022b).

Following ISO standards and the EU Product Environmental Footprint requirements for LCA assessments, the key impacts were analyzed across ten categories, including Abiotic depletion, Acidification, Eutrophication, Freshwater aquatic ecotoxicity, Global warming (GWP100a), Human toxicity, Marine aquatic ecotoxicity, Ozone layer depletion (ODP), Photochemical oxidation, and Terrestrial ecotoxicity. The research employed a midpoint LCA modeling method for analyzing the parameters of each stage and an endpoint method for examining the overall process (Pons et al., 2018).

The assessment units have been chosen accurately and sensibly, and the case structures are composed of a mixture of materials with intricate interfaces, including cable-stayed bridges and suspension bridges (Kim et al., 2017; Deeney et al., 2021). Using Kg as the unit of evaluation for complex variable-section structures is appropriate.

$$\sum_{i=\text{Design}}^{j=\text{Construction}} E_{\text{T}}(\bar{x}, T_{\text{Stage}}) = \sum_{T_1=S}^{T_{i_1}=F} E_{\text{Design}}^{\text{T}}(x_d) \cup \sum_{T_2=S}^{T_{i_2}=F} E_{\text{Material}}^{\text{T}}(x_m) \cup \sum_{T_3=S}^{T_{i_3}=F} E_{\text{Construction}}^{\text{T}}(x_c) \quad (4)$$

$\sum_{i=\text{Design}}^{j=\text{Construction}} E_T(\bar{x}, T_{\text{Stage}})$ are three stages of environmental impact data of the bridge (kg); $\bar{x}, T_{Stage}$ are the set of impact variables corresponding to each stage; $\sum_{T_1=S}^{T_i=F} E_{\text{Design}}^T(x_d)$ is environmental impact value at the design stage (kg); $\sum_{T_2=S}^{T_i=F} E_{\text{Material}}^T(x_m)$ is environmental impact value at the material stage (kg); $\sum_{T_3=S}^{T_i=F} E_{Construction}^T(x_c)$ is environmental impact value at the construction stage (kg); S = Start; F = Finished; T = Total.

The environmental impact of each stage is directly related to personnel, materials, machinery, operating environment, and operating scheme. Eq (3) is optimised (Liu and Qian, 2019).

$$\sum_{T_1=S}^{T_{i_1}=F} E_{\text{Design}}^T(x_d) = \sum_{T_1}^{T_{i_1}} E_{\bar{P}=p_{\text{Number}}/T}^T(x_p) + \sum_{T_1}^{T_{i_1}} E_m^T(x_m) + \sum_{T_1}^{T_{i_1}} E_e^T(x_e) + \sum_{T_1}^{T_{i_1}} E_c^T(x_c) + \sum_{T_1}^{T_{i_1}} E_s^T(x_s) \quad (5)$$

$\sum_{T_1}^{T_{i_1}} E_{\bar{P}=p_{\text{Number}}/T}^T(x_p)$ is personnel environmental impact value (kg); $\bar{p}$ is average deviation of number of people at the design stage (person-time); $\sum_{T_1}^{T_{i_1}} E_m^T(x_m)$ is environmental impact value of used materials (kg); $\sum_{T_1}^{T_{i_1}} E_e^T(x_e)$ is environmental impact value of equipment and machinery (kg); $\sum_{T_1}^{T_{i_1}} E_c^T(x_c)$ is environmental impact value of operating conditions (kg); $\sum_{T_1}^{T_{i_1}} E_s^T(x_s)$is environmental impact value of operating schemes and methods (kg).

Life cycle cost (LCC): LCC of engineering structures refers to total costs generated within the life cycle of structures, including costs of design, construction, inspection, maintenance, repair, and failure (Z. Wang et al., 2020).

$$\text{LCC} = C_r + C_{pm} + C_{ins} + C_{rep} + C_f + C_d \quad (6)$$

C_r is initial cost (CNY); C_{pm} is daily maintenance cost (CNY); C_{ins} is inspection cost (CNY); C_{rep} is repair cost (CNY); C_f is expected failure cost (CNY); C_d is disassembly cost (CNY).

The software used for conducting social impact assessments (SIA) is OpenLCA 1.10.3, and it draws data from a variety of sources, including the Product Social Impact Life Cycle Assessment (PSILCA), USDA data, and the Social Hotspots Database (SHDB) (Z. Zhou et al., 2021). OpenLCA is a mature software that seamlessly integrates LCC, Life Cycle Assessment (LCA), and SIA with different functional units, discrete variables, and multiple databases. This has earned its official recognition from ISO14040 (Zeug et al., 2021).

Wang et al. (Y. Wang et al., 2021) conducted a study on the social impact of the civil construction industry, dividing it into two levels and categorizing it using six classification indicators. They found that social impact can be achieved through sustainable digital development, allowing readers to make informed judgments and conclusions based on data and to progress from qualitative understanding to quantitative standards.

$$C_S = SC_{PHY}+SC_{PSY}+SC_{PE}+SC_{HS}+SC_{SE}+SC_{SR} \tag{7}$$

C_S is total social costs of the civil construction industry; SC_{PHY} is the social costs of overall physical impacts ; SC_{PSY} is the social costs of psychological impacts; SC_{PE} is the social costs in terms of overall personal economic losses; SC_{HS} is the overall social cost for human settlement; SC_{SE} is the overall social costs concerning socioeconomic conditions; SC_{SR} is the social costs induced by loss of social resources.

2.3. Principles of algorithms programs

Three methods are commonly utilized for regional economic analysis: the econometric model, the input-output model, and the computable general equilibrium model (Kennedy et al., 2004). The connection between transportation, location, and economic development is complex, as numerous factors influence infrastructure investment and construction. To effectively determine and evaluate this relationship, the analysis must begin at its foundational level (Yang et al., 2018). This research selects bridges in the four regions with the most robust economies as its case study objects, aiming to enhance the robustness of LCA and SIA analysis and to evaluate and analyze regional sustainable development.

Zhou et al. (Z.W. Zhou et al. 2022b) investigated the correlation between economic development and transportation driving factors using Ordinary Least Squares Regression (OLS) and Geographically Weighted Regression (GWR). They developed separate regression equations to assess the non-stationary relationship between dependent and independent variables (Zamarrón-Mieza et al., 2017).

$$y_i = \beta_0(u_i, v_i)+\sum_{i=1}^{k}\beta_k(u_i, v_i)x_{ik}+\varepsilon_i \tag{8}$$

y_i is estimated value of comprehensive economic indicators; $\beta_0(u_i, v_i)$ is expresses the intercept for i; $\beta_k(u_i, v_i)$ is the local parameter estimate for independent variable x_k at location i.

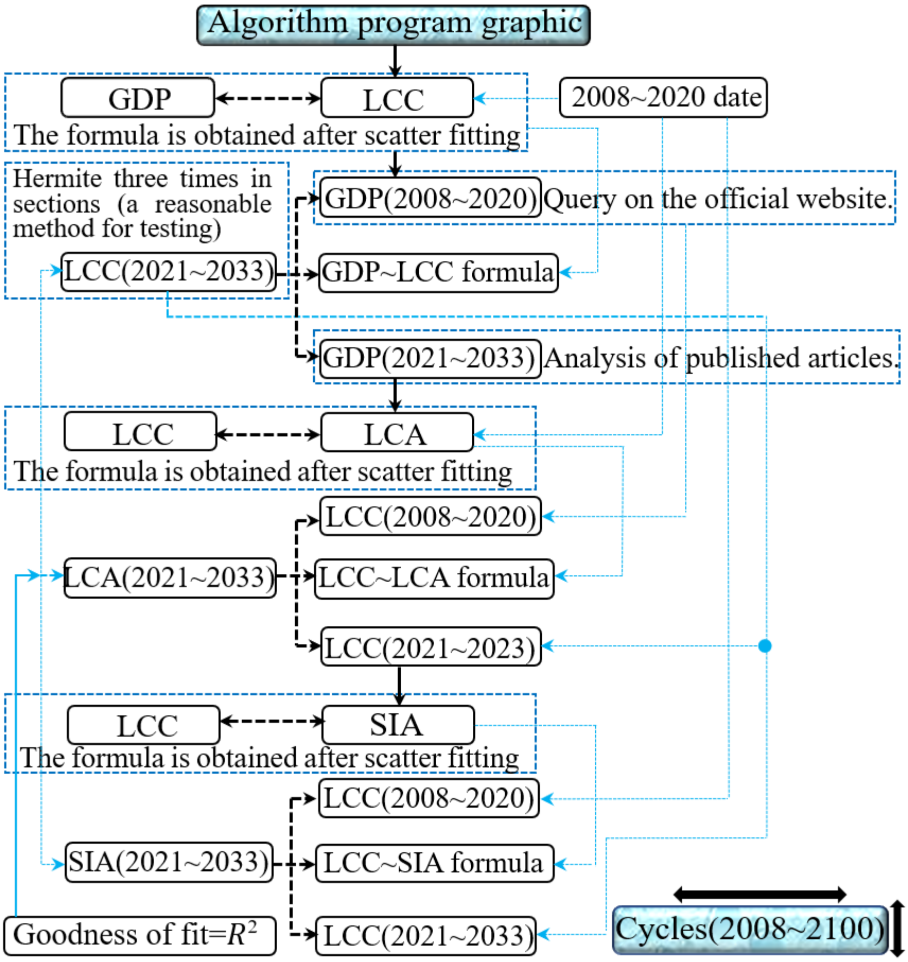

Fig. 3. Logic programming of scientific algorithm language programs.

2.4. Model of scientific algorithm

Applying computer programs and the theoretical model of advanced mathematics can effectively solve the complexity and discreteness problems of the influencing factors of construction industry assessment, significantly improving the reliability and accuracy of research results (Z. Zhou et al., 2021). This research employs the data interpolation calculation mechanism (the principle of function approximation) (Rohner and Kjellerstrand, 2021):

Data has been obtained: x_1, x_2, ⋯ , x_n ; y_1 , y_2, ⋯ , y_n. Build functional Eqs: $y = f(x)$. create new function: $Ø(x) = f(x)$, Satisfy $Ø(x_i) = y_i$ $(i = 1, 2, 3, \cdots, n)$. $Ø(x)$ is an approximate approximation function of y. After the new value of x_i is determined, the new data y_i can be obtained by using $Ø(x_i)$ (the approximation function is applied to obtain the interpolated data).

Four kinds of interpolation function models are commonly used: linear; nearest point; piecewise cubic Hermitian; cubic spline interpolation fitting (Fig. 4).

$$\sum y_i \rightarrow \begin{cases} y_1 = \text{interpi}(x, y, x_1, \text{linear}) & \text{Determine vector of } x, y \quad \text{Interpolate data } of \ x_1 \\ y_1 = \text{interpi}(x, y, x_1, \text{nearest}) & \text{Determine vector of } x, y \quad \text{Interpolate data } of \ x_1 \\ y_1 = \text{interpi}(x, y, x_1, \text{pchip}) & \text{Determine vector of } x, y \quad \text{Interpolate data } of \ x_1 \\ y_1 = \text{interpi}(x, y, x_1, \text{spline}) & \text{Determine vector of } x, y \quad \text{Interpolate data } of \ x_1 \end{cases} \tag{9}$$

Fig. 3 displays the scientific algorithm model for sustainable development. The program performed inference and calculation of LCC, LCA, and SIA variable data from 2008 to 2100, and the research conclusion was arrived at by analyzing the procedural memory module（Cole and McCrea, 2016).

Language symbol sees 4.2 for the computer programming language running program.

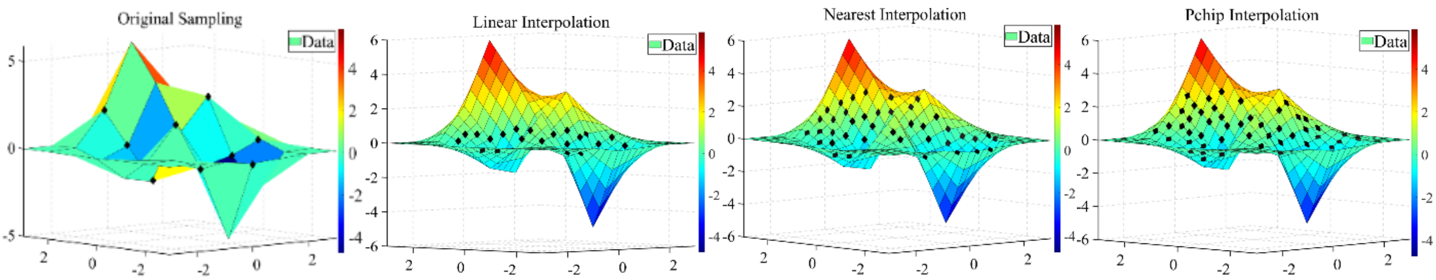

(a) (b) (c) (d)

Fig. 4. Four mathematical approximation models: (a) The original function. (b) Linear. (c) Nearest point. (d) Piecewise cubic Hermitian.

3. Results

A high-quality case research is a well-established method in innovation research. Goffin et al. (Goffin et al., 2019) analyzed 818 case studies published in the past 20 years. The proposed standards for selecting high-quality case studies, including an appropriate research design, effective data collection, thorough data analysis, and accurate post-study analysis.

This research uses bridges in four major economic regions as primary data: Hanjiang Bridge (XHJ1, Fig. 5a); Mu Gao Bridge (SXM2, Fig. 5b); Wang Lan Bridge (WLT3, Fig. 5c); Jin Ma Bridge (JMD4, Fig. 5d).

Long-span cable-stayed bridges are characterized by their large size, intricate structures, numerous interconnec -ting components, and diverse materials. The presence of uncertain parameters poses challenges to finite element model research, but a high-fidelity finite element model helps enhance the research's robustness (Cai et al., 2020). These bridges serve as municipal road bridges designed to meet the load requirements specified by *JTGD60-2015* following construction industry standards (China, 2015).

3.1. Analysis of load

As indicated in the design documents and code standards (refer to Table 2), the forces acting on the four cable-stayed bridges are composed of permanent and variable actions. The permanent actions include structural gravity, pre-applied force, concrete shrinkage and creep, water buoyancy, and total displacement. The variable actions consist of loads from vehicles, vehicle impact, centrifugal force, braking force, crowds, fatigue, wind, water pressure, temperature variations, and bearing friction resistance (Sun et al., 2020).

Table 2

Statistics on the applied loads of the four bridges.

Name (N/m²)	XHJ1		SXM2		WLT3		JMD4	
	Main structure	Basic part	Main structure	Basic part	Main structure	Basic part	Main structure	Basic part
Structural gravity	65,389.91	160.21	316,317.41	218,052.01	43,810.09	2,430.88	3,475.79	550.87
Water buoyancy	0.32		0.18		0.69		6.81	
Carload	34,330		34,330		34,330		34,330	
Car impact	15,448.5		15,448.5		15,448.5		15,448.5	
Car centrifugal force	The bridge line is within the straight line.							
Car braking force	4,200		2,100		2,100		4,200	
Crowd load	0		2,500		2,500		0	
Fatigue load	3,150		3,150		3,150		3,150	
Wind load	See Calculation part.							
Bearing friction	0.3w (w= Gravity above the bearing pad stone)							

3.2. Analysis of finite element

The three-dimensional concrete constitutive model can effectively evaluate changes in core stress, strain, structural deformation, and energy and precisely predict the peak value of the curve. The aim is to identify the best structure that satisfies both the design requirements and the manufacturing constraints (Shobeiri and Ahmadi-Nedushan, 2017). The finite element mesh density analysis of XHJ1, SXM2, WLT3, and JMD4 was performed with a suitable unit length. The finite element analysis of the entire bridge exhibits high accuracy and efficiency (Briseghella et al., 2016). The XHJ1 grid was divided into 167,290 groups with 0% error in mesh generation and a warning set of 16.54% of the total. The SXM2 grid was divided into 169,487 groups with no error and a warning set of 0.596% of the total. The WLT3 grid was divided into 133,951 groups with 0% error and a warning set of 4.390% of the total. The JMD4 grid was divided into 350,109 groups with 0% error and a warning set of 18.852% of the total. Accurate mesh division lays the foundation for three-dimensional coupled topology optimization analysis.

After performing finite element deformation analysis on the components, the focus shifts to two key performance indicators: structural stiffness and strength (energy) and deformation (displacement). These indicators play a critical role in determining the quality and stiffness design of the bridge and represent a shift in production and design philosophy (Reintjes and Lorenz, 2021).

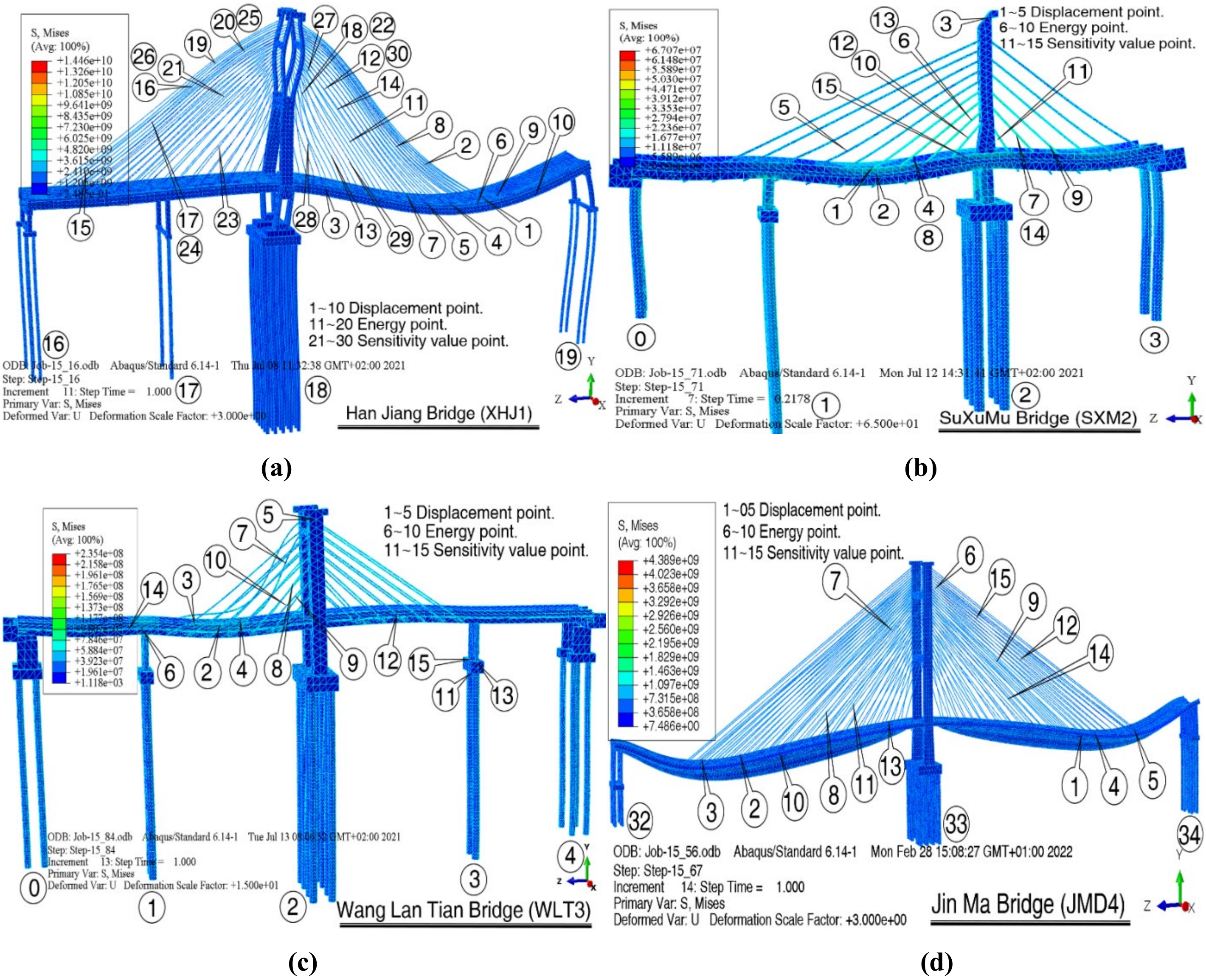

Fig. 5. Finite element analysis, a-d: (a) XHJ1. (b) SXM2. (c) WLT3. (d) JMD4.

The XHJ1 structure was analyzed using twelve groups of elements for each sub-structure of 16#, 17#, and 19#, resulting in 34 groups. This analysis was performed to determine the discreteness of the influencing factors, with XHJ1 having a capacity of 176 elements. The ranking of total bridge displacement and energy was calculated using the XHJ1 data (as shown in Fig. 6a). The structural stability of XHJ1 was determined by calculating the SRSW using Eq (3). The whole bridge Q_c ranking (Figs. 5a, 6b). The numerical values of Q_c were used to determine the sequence of structural stability of XHJ1, and it was found that 16#, 17#, and the girder have conditions of TO.

The SRSW, calculated using Eq (3), was found to align with the Shape-preserving (P chip) interpolant analysis, as shown in Fig. 6b. The research revealed that the elements experiencing maximum displacement and energy changes do not coincide with the elements in the SRSW region. These findings emphasize the importance of analyzing the SRSW region before examining the maximum stress and structural ultimate bearing capacity in structural design and dynamic studies.

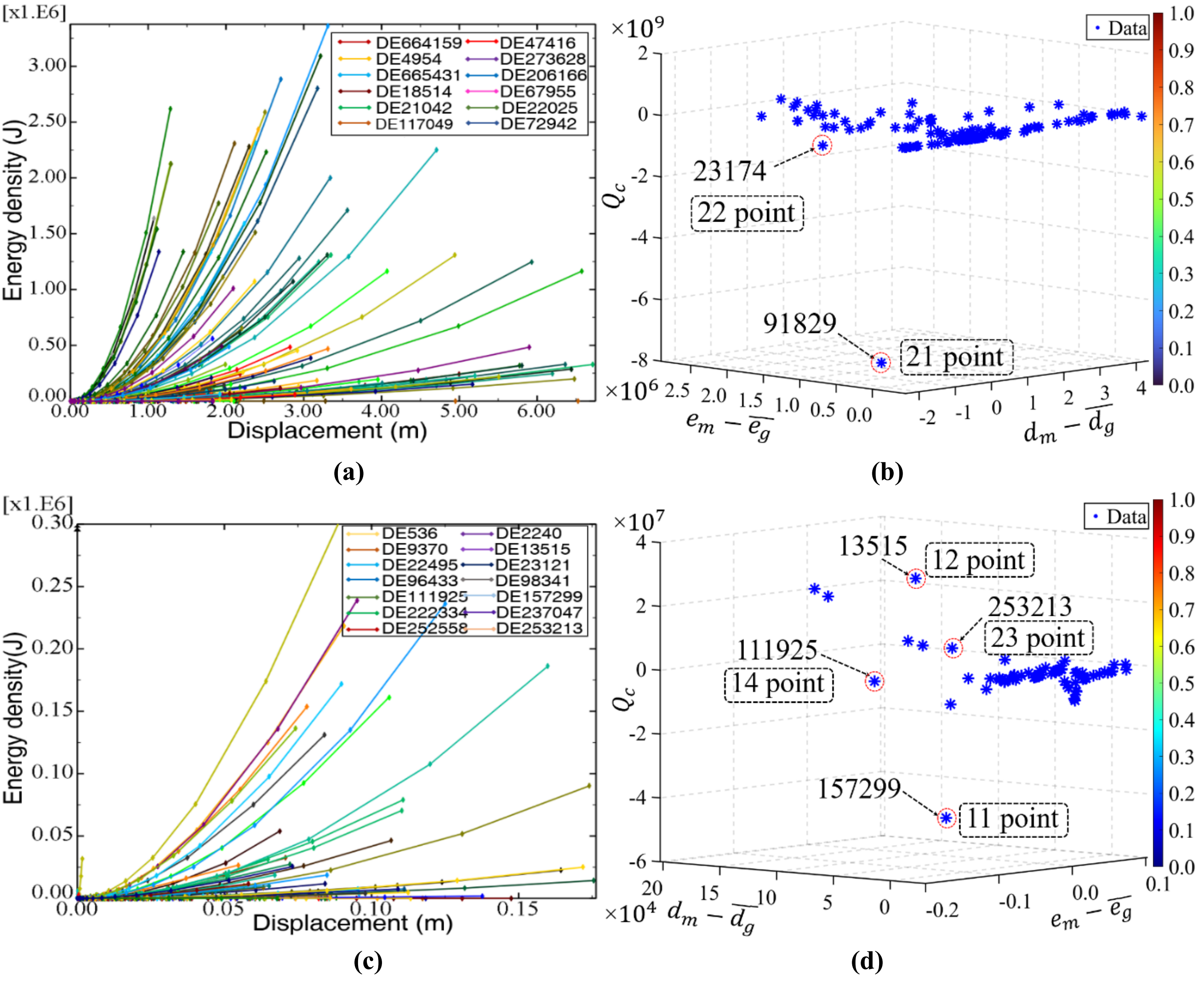

Fig. 6. Finite element analysis a-d: (a) Schematic diagram of displacement and energy of acquisition points after XHJ1 topology coupling. (b) Q_c analysis of XHJ1. (c) Schematic diagram of displacement and energy of acquisition points after SXM2 topology coupling. (d) Q_c analysis of SXM2.

In the finite element analysis of SXM2, 72 groups of elements were observed, including two groups with zero-point energy values. The rankings of displacement and energy were calculated and presented in Fig. 6c. SRSW: The full- bridge Q_c ranking was calculated for SRSW and shown in Figs. 5b, 6d. Based on these values, the sequence of determining SXM2 was found to be as follows: preliminarily, 00#, 01#, and 02# were determined to have conditions of TO.

In the finite element analysis of WLT3, 84 groups of elements were observed. The cable area concentrated the maximum displacement, as reflected in the displacement and energy rankings presented in Fig. 7a. The observation points showed that the maximum strain energy of the bridges was discrete, which is favourable for TO. The WLT3 ranking of Q_c was calculated and presented in Figs. 5c, 7b. Based on these values, it was preliminarily determined that 0#, one#, and two# have conditions of TO.

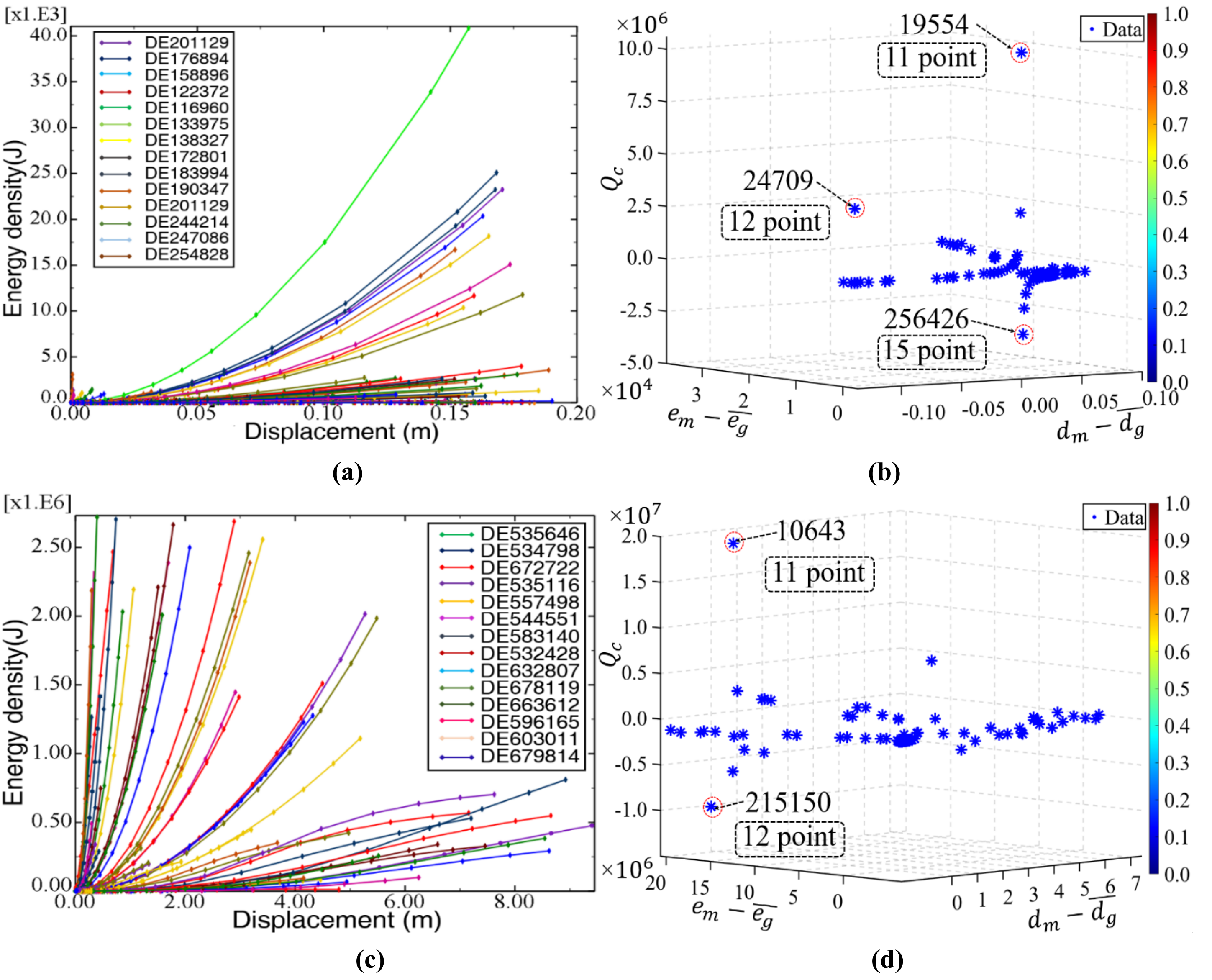

Fig. 7. Finite element analysis a-d: (a) Schematic diagram of displacement and energy of acquisition points after WLT3 topology coupling. (b) Q_c analysis of WLT3. (c) Schematic diagram of displacement and energy of acquisition points after JMD4 topology coupling. (d) Q_c analysis of JMD4.

During the analysis of JMD4, 105 groups of elements were observed. The displacement and energy rankings are displayed in Fig.7c. The JMD4 ranking of Q_c was calculated and presented in Figs. 5d, 7d. The analysis of calculation parameters revealed that 34#, the girder, and 33# have conditions of TO in JMD4.

Table 3

Response data of sensitive indicators of the four bridge structures.

`	Part		Interval	Name	Part		Interval
XHJ1	16#	445,645.9	Max=-7,843,690,464.88;Min=-33,446.12	WLT3	0#	-38,244.65	Max=-7,843,690,464.88;Min=33,446.12
	17#	445,581.1			1#	-126,280.6	
	Girder	45,738.85			2#	-64,685.03	
SXM2	00#	519,253.2	Max=-7,843,690,464.88;Min=33,446.13	JMD4	33#	336,145.03	Max=-7,843,690,464.88;Min=33,446.12
	1#	-401,152			34#	336,145.03	

3.3. Analysis of topology optimization

The fluctuation quantity in four bridges, as analyzed in the finite element and the TO design, is determined in Table 3. The XHJ1-16# underwent two rounds of TO design. The initial volume was set to 90% in the first design and reduced by 10% over 14 design cycles. However, the main structure of the 16# tie beam and cross girder sustained damage, causing the TO design to fail. The second design was set to 95% with a 5% reduction, and the main structure remained undamaged. The results show that within the interval range of 2,939,383,740 > Q_c > -1,009,563.877 (Table 3), the TO design was successful (Fig. 8a).

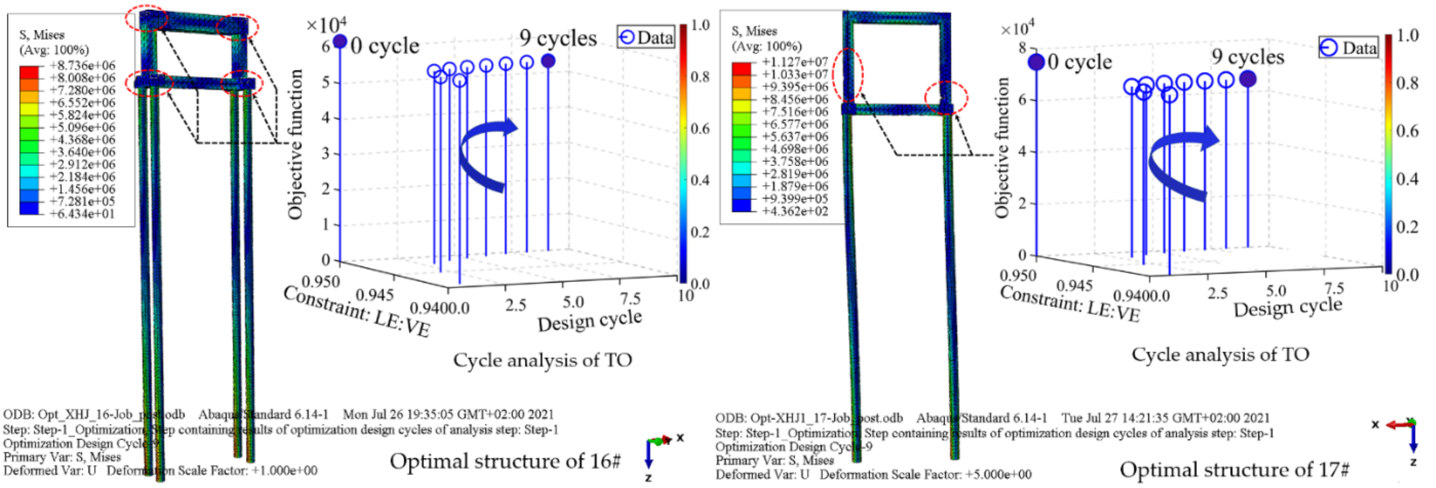

(a) **(b)**

Fig. 8. TO of bridge: (a) XHJ1-16#. (b) XHJ1-17#.

The XHJ1-17# underwent topology optimization analysis with an initial design volume of 90% and a reduction of 10%. The analysis showed that the interval range was 99,420,983.57 > Q_c > -22,828,721.21 (Table 3), outside the determined numerical range. The main structure of the 17# pier column sustained damage, leading to the failure of the first TO design. A second design with a volume of 95% and a reduction of 5% was conducted. The results showed that 175,979,565.1 > Q_c > 6,826,036.43 complied with Table 3. The main structure was not damaged, and the TO design was successful (Fig. 8b). Unfortunately, the main beam of XHJ1 was damaged-during the optimization process, causing the TO design to fail.

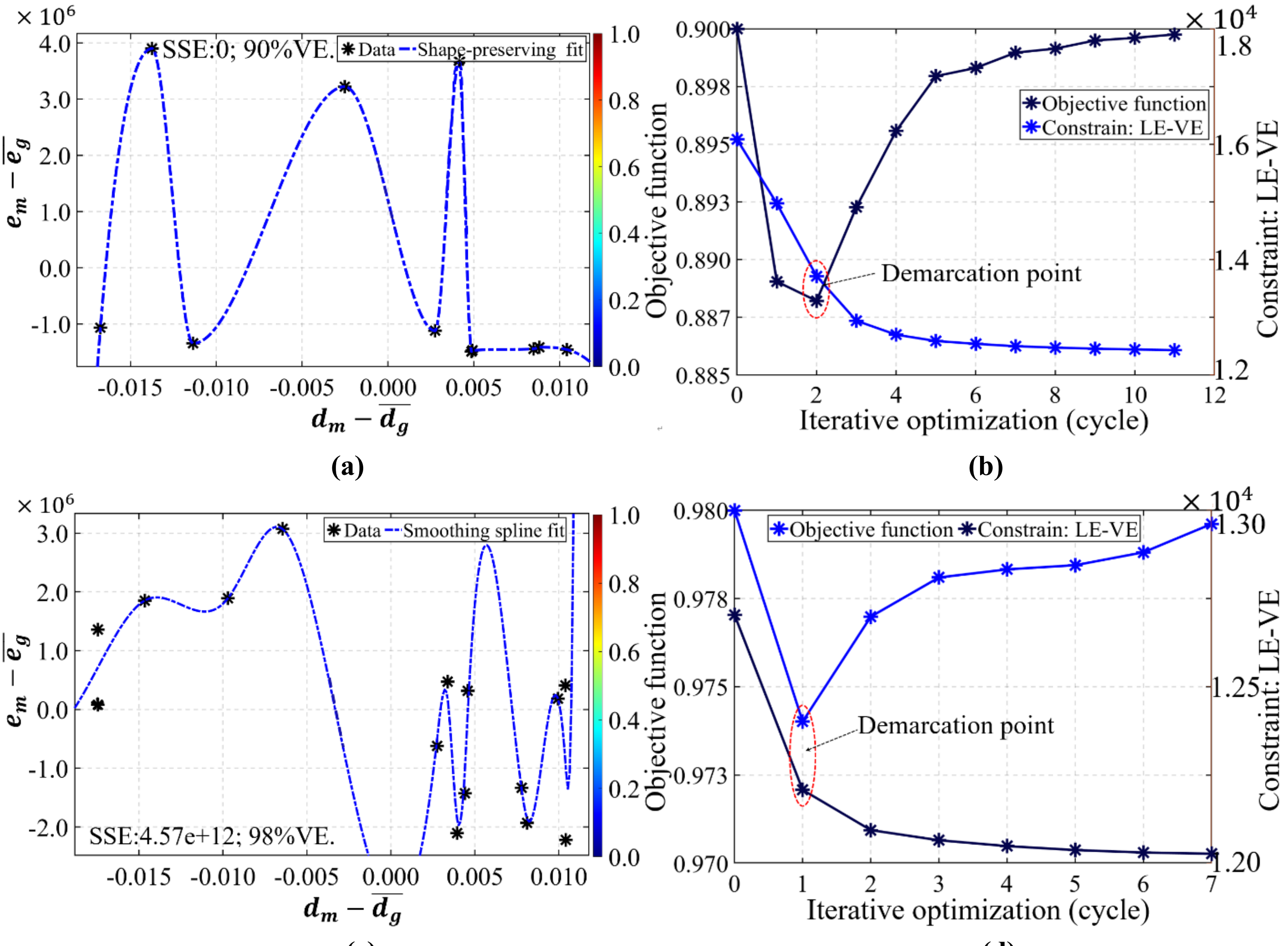

Fig. 9. Thin-plate spline interpolant analysis, a-d: (a) 90% of SXM2-0#. (b) Cycle analysis of 90% TO. (c) 98% of SXM2-0#. (d) Cycle analysis of 98% TO.

The SXM2-0# underwent design with the volume set at 90%, 95%, and 98%. All elements met the best-fit condition of the structure SSE and had a numerical value R that followed a discrete distribution (Cole and McCrea, 2016). The conclusion was that the 0# had no redundant structures in the TO design (Table 4).

The SXM2-1# underwent design with the volume set at 90%, 95%, and 98%. However, the TO design failed on all three occasions. The conclusion was that the 1# could not be optimized through TO design. Similarly, the SXM2-2# underwent design with the volume set at 90% and 95%. Despite the attempts, the TO design failed twice, and the conclusion was that the 2# could not be optimized through the TO design process (Table 4).

The WLT3-0# underwent design with the volume set at 90% and 96%. However, the TO design failed on both occasions. The conclusion was that the 0# could not be optimized through TO design. Similarly, the design volume of WLT3-1# was set at 90% and 96%, and the TO design failed twice. The conclusion was that the 1# also could not be optimized. Both 0# and 1# were found to have no redundant structures in the TO design (Table 4).

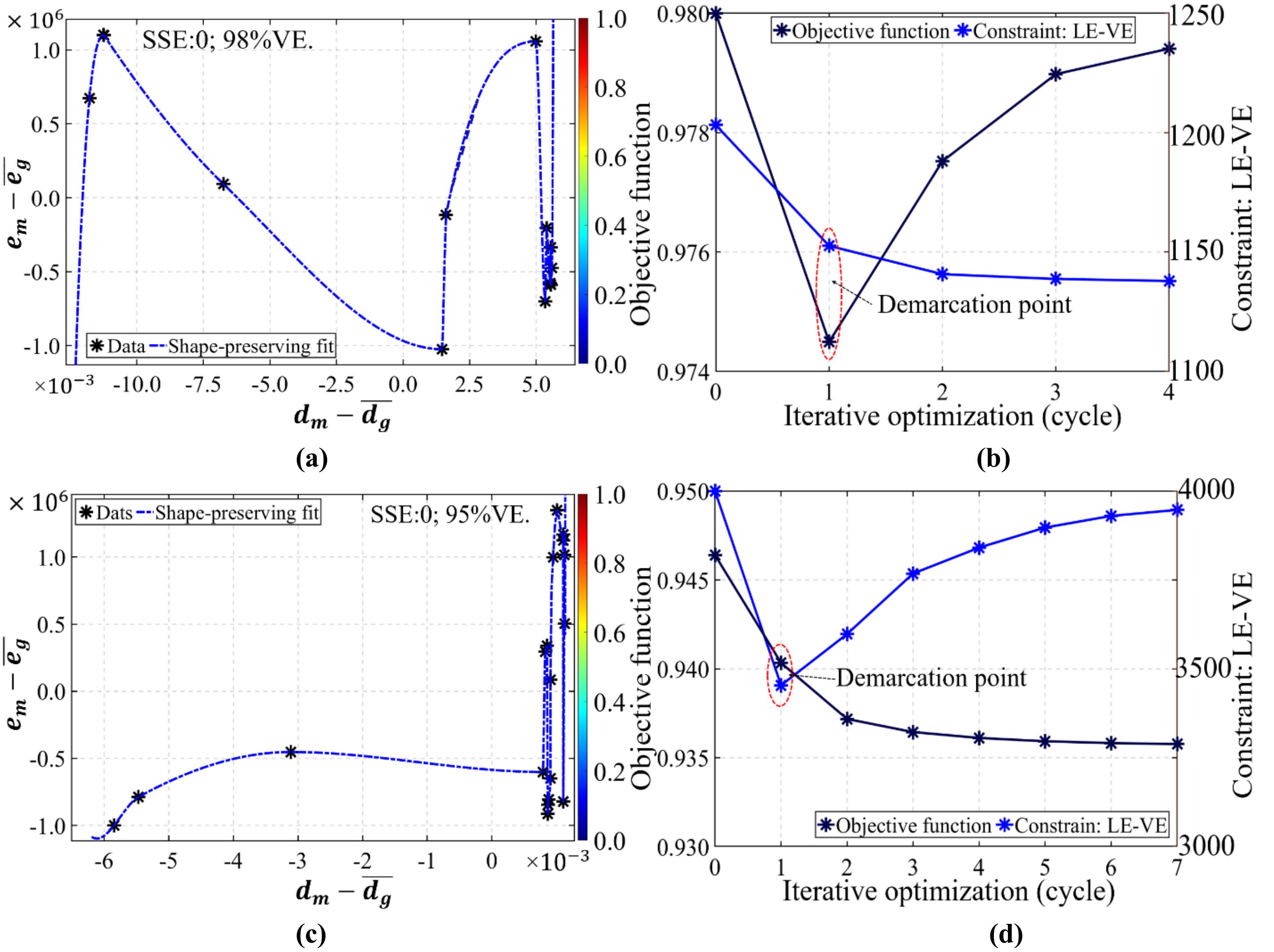

Fig. 10. Thin-plate spline interpolant analysis, a-d: (a) 98% of SXM2-1#. (b) Cycle analysis of 98% TO. (c) 95% of SXM2-2#. (d) Cycle analysis of 95% TO.

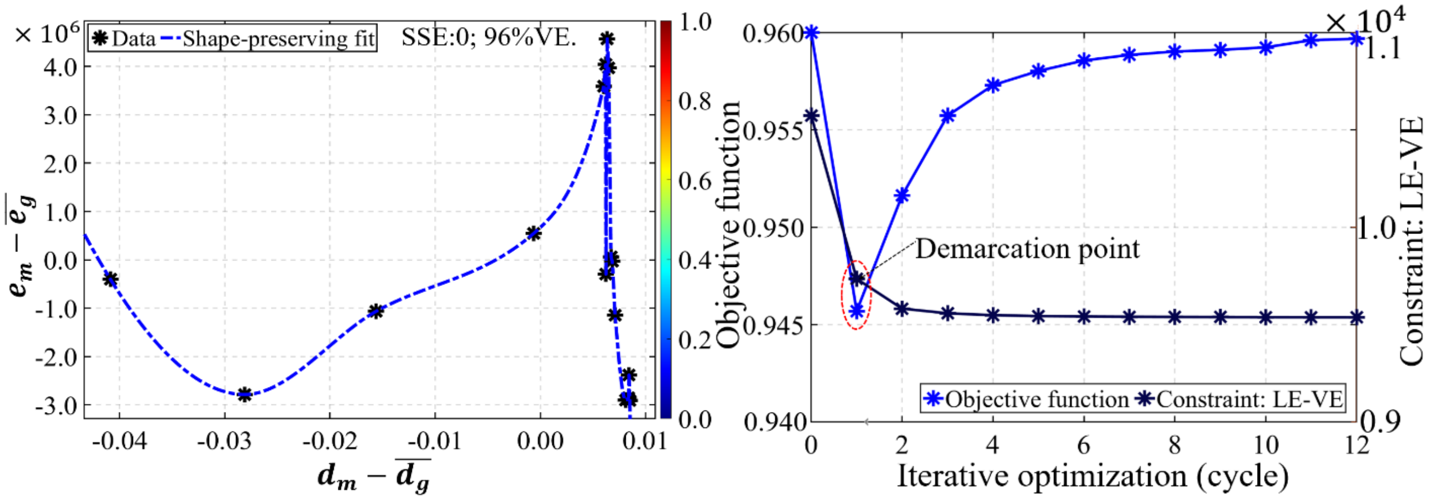

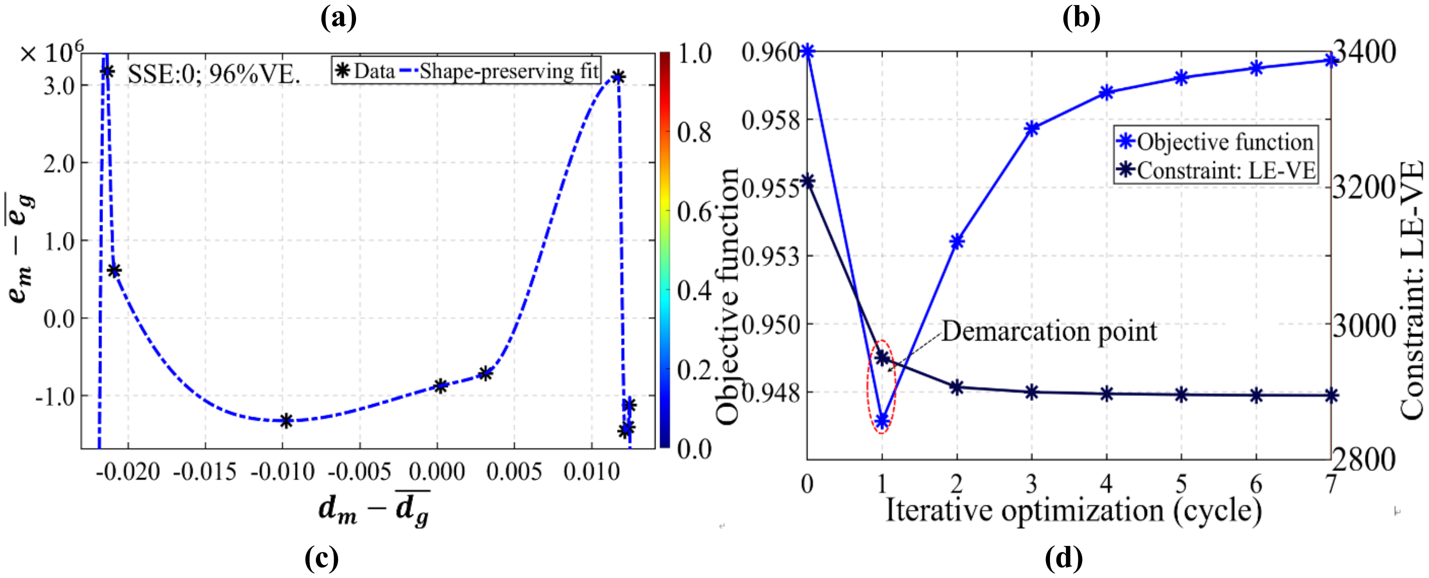

Fig. 11. Thin-plate spline interpolant analysis, a-d: (a) 96% of WLT-0#. (b) Cycle analysis of 96% TO. (c) 96% of WLT-1#. (d) Cycle analysis of 96% TO.

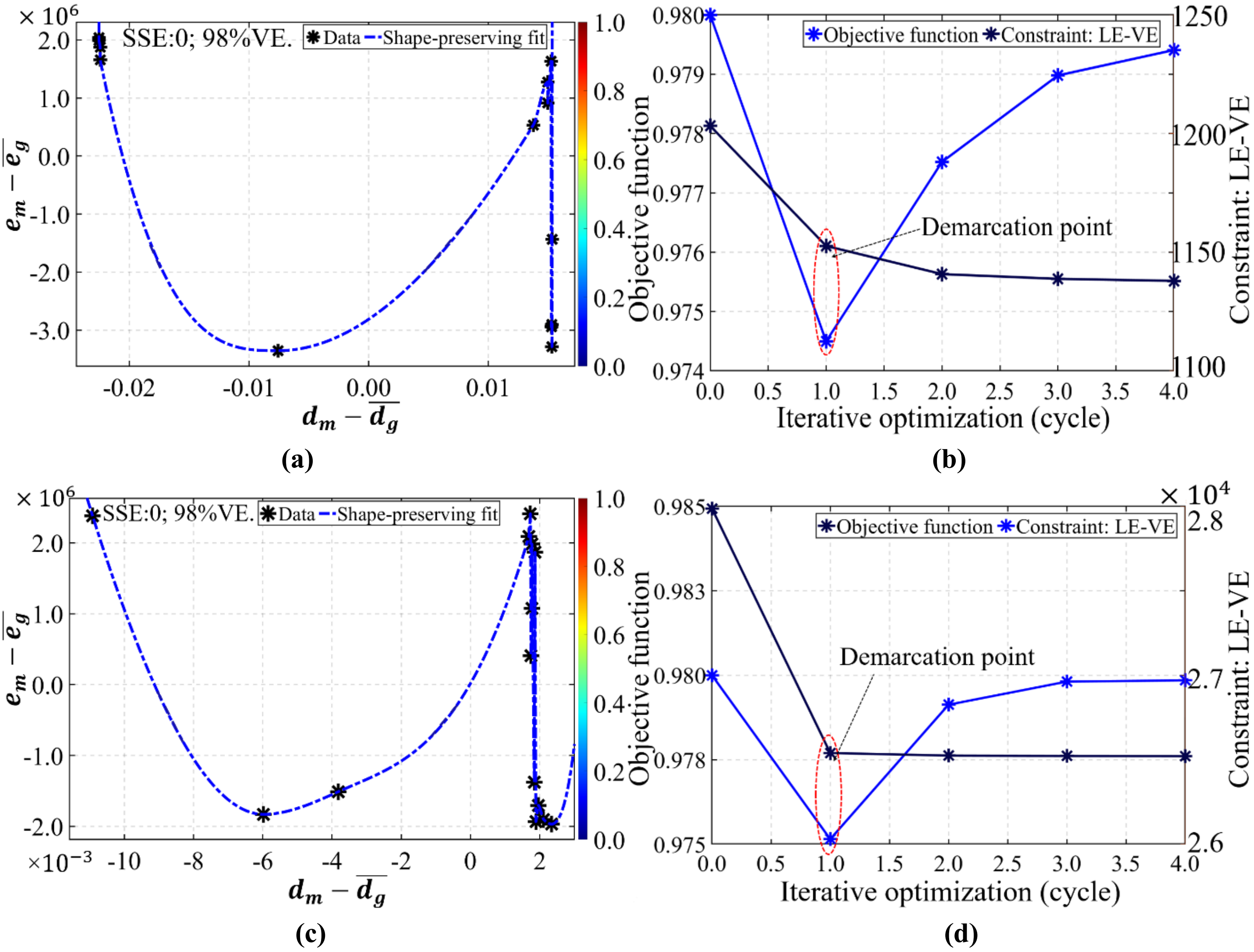

Fig. 12. Thin-plate spline interpolant analysis, a-d: (a) 98% of JMD-33#. (b) Cycle analysis of 98% TO. (c) 98% of JMD-34#. (d) Cycle analysis of 98% TO.

JMD4: The design volume of JMD4-33# was set as 85%, 98%. The TO failed two times.33# does not have a redundant structure. The design volume of JMD4-34# was set as 90%, 98%. The TO failed two times. 34# does not have a redundant structure (Table 4).

As shown in Table 4, the TO of four bridges showed that the volume of XHJ-16# and 17# was reduced by 5%, while the other bridge structures were found to have no redundant systems, as calculated based on the original design.

Table 4

TO data of four bridge structures.

Name	Precent of volume	Design cycles	Damage of structure	Q_c	Conclusion
XHJ1_16	90%	13 Times	×	178,654,983 > Q_c > -684,532.55	× (Fig. 8a)
	95%	9 Times	√	2,939,383,740 > Q_c > -1,009,563.877	√ (Fig. 8a)
XHJ1_17	90%	10 Times	×	99,420,983.57 > Q_c > -22,828,721.21	× (Fig. 8b)
	95%	9 Times	√	175,979,565.1 > Q_c > 6,826,036.43	√ (Fig. 8b)
SXM2_0	90%	11 Times	×	1,281,345,494 > Q_c > 63,664,657.35	× (Figs. 9a, b)
	95%	9 Times	×	-3,244,522,815 > Q_c > 8,284,317.5	×
	98%	7 Times	×	-532,452,933.6 > Q_c > -4,506,263.36	× (Figs. 9c, d)
SXM2_1	90%	13 Times	×	270,388,142.4 > Q_c > -14,520,301.12	×
	95%	8 Times	×	780,643,151.1 > Q_c > -1,517,586.43	×
	98%	4 Times	×	-701,288,436.8 > Q_c > -37,998,850.71	× (Figs. 10a, b)
SXM2_2	90%	10 Times	×	-4,634,604,579 > Q_c > -27,256,726.73	×
	95%	7 Times	×	1,334,615,139 > Q_c > 144,044,733.5	× (Figs. 10c, d)
WLT3_0	90%	11 Times	×	1,432,123,203 > Q_c > -42,437,380.68	×
	96%	12 Times	×	-845,091,381 > Q_c > -4,718,338.54	× (Figs. 11a, b)
WLT3_1	90%	11 Times	×	37,425,803.26 > Q_c > -140,768,894.4	×
	96%	7 Times	×	-29,360,860.81 > Q_c > -41,183,79,789	× (Figs. 11c, d)
JMD4_33	85%	10 Times	×	297,163,264.2 >Q_c > 15,333,066.07	×
	98%	4 Times	×	442,588,455.5 > Q_c > 38,815,691.75	× (Figs. 12a, b)
JMD4_34	90%	11 Times	×	1,115,702,200 > Q_c > -222,240,829.2	×
	98%	4 Times	×	1,394,539,726 > Q_c > -218,133,773.9	× (Figs. 12c, d)

Notes: × indicates that the primary structure was damaged; √mains the primary structure is intact. Q_c is the sensitivity weight of structural response; After completing the topology optimization analysis of the selected components of the four bridges, the author needs to measure the Q_c value, which will be used as one of the criteria for judging the success of the topology optimization.

4. Discussion

The optimum structure model of four bridges was determined (Table 4; Fig. 13). The research conclusion shows that the four bridge paradigms are all successful.

Table 5
LCA data of four bridge structures.

Indicator	Unit (Index: eq)	XHJ1	SXM2	WLT3	JMD4
Abiotic depletion	t Sb	242.00	7.08	7.73	327.00
Acidification	t SO2	181.00	5.23	5.00	342.00
Eutrophication	t PO4	57.40	2.40	0.277	120.00
Fresh water aquatic ecotax	t 1,4-DB	19,700.00	792.00	375.00	38,100.00
Global warming	t CO2	41,100.00	1,410.00	1,730.00	57,500.00
Human toxicity	t 1,4-DB	36,300.00	2,210.00	1,060.00	117,000.00
Marine aquatic ecotoxicity	1000 t, 1,4-DB	42,700.00	1,300.00	2,090.00	82,900.00
Ozone layer depletion	kg CFC-11	3.10	0.09	0.08	3.65
Photochemical oxidation	kg C2H4	16,900.00	604.00	520.00	23,100.00
Terrestrial ecotoxicity	t 1,4-DB	282.00	9.22	5.03	422.00

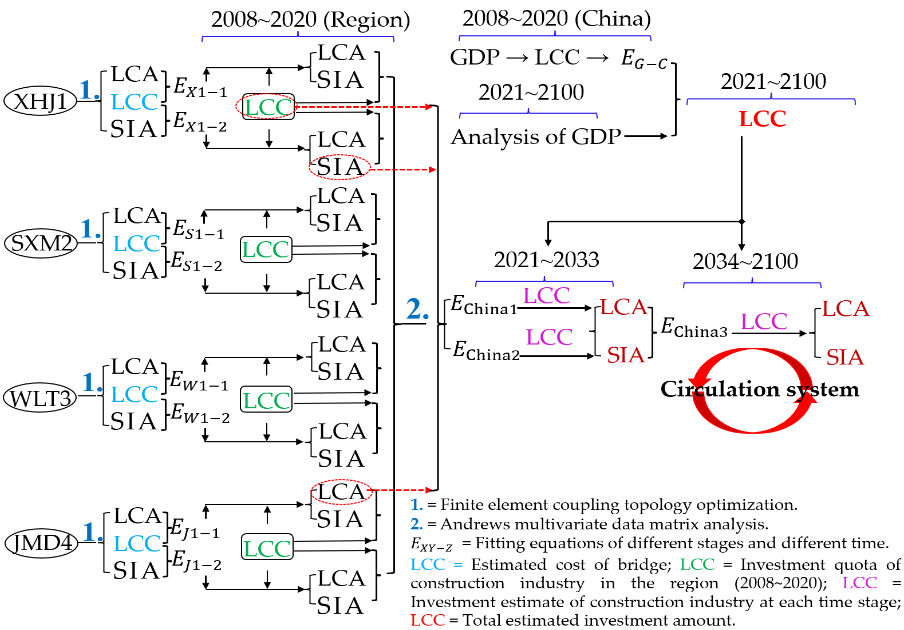

Fig. 13. Fitting analysis system model.

The LCA analyzed the parameters that affect it through the software OpenLCA (Table 5). The XHJ1, SXM2, and JMD4 processes and process links are numbered 9929 and 92785, 10100 and 94353, 9939 and 92777, respectively. The total LCA values showed JMD4 with the highest value at 83,125,664.74 tons, followed by XHJ1 (42,769,149.29 tons), WLT3 (2,097,392.48 tons), and SXM2 (1,303,153.65 tons). The most significant impact category was marine aquatic ecotoxicity, accounting for 99.77%, 99.66%, 99.85%, and 99.74% of total emissions releases. The research data indicates that human activities significantly impact marine environmental quality and ecosystem changes, highlighting the importance of considering the heterogeneous impact of land on marine ecology (Z. Wang et al., 2020).

The LCC analysis was performed on road bridges using the financial analysis method outlined in relevant engineering budget standards (*JTG/T3365-01-2020*; *JTGD60-2015*; *JTG/T3820-2018*; *JTG/T3821-2018*; and

JTG/T3832-2018) (Rohner and Kjellerstrand, 2021). The results, as shown in Table 6, indicate that the construction costs for the four bridges were JMD4 (70,283,672.8CNY) > XHJ1 (47,405,917.99CNY) > SXM2 (22,692,076.15CNY) > WLT3 (6,024,637.837CNY).

Table 6

LCC data of four bridge structures.

Project	Name	XHJ1	SXM2	WLT3	JMD4
1	Direct fee	41,156,098.63	18,860,946.38	3,824,713.76	61,794,857.67
2	Insurance	1,234,682.96	565,828.39	114,741.41	1,853,845.73
3	Completion and environmental protection fees	1,500,000.00	1,500,000.00	1,500,000.00	1,500,000.00
4	Safety production fee	617,341.48	282,914.20	57,370.71	926,922.87
5	Management information fee	200,000.00	200,000.00	200,000.00	200,000.00
6	Temporary road, land occupation	168,740.00	77,329.88	15,681.33	253,358.92
7	Temporary power supply and communication	65,849.76	30,177.51	6,119.54	98,871.77
8	Water supply and sewage facilities	32,924.88	15,088.76	3,059.77	49,435.89
9	Standard chemical field construction	172,855.61	79,215.97	16,063.80	259,538.40
10	Provisional amount	2,257,424.67	1,080,575.05	286,887.52	3,346,841.56
	Estimated total price	47,405,917.99	22,692,076.15	6,024,637.84	70,283,672.80

SIA: Zhou et al. (Z.W. Zhou et al., 2020) studied the environmental impact of cable-stayed bridges and developed data models based on 18 influencing parameters. The data analysis was performed using these 18 parameters. Table 7 presents the results of the analysis for the four bridges. The highest emissions in the SIA value were in marine ecotoxicity and human toxicity, while the lowest was in the ozone depletion category. The total SIA values were JMD4 (3,728,938,758) > XHJ1 (1,243,367,222) > WLT3 (250,341,322.8) > SXM2 (53,709,600.26).

Table 7

SIA data of four bridge structures.

Name	Unit (Index: eq)	XHJ1	SXM2	WLT3	JMD4
Gender wage gap	t u235	1,950.00	81.90	72.80	2,350.00
Child labor, female	t	940.00	28.30	24.10	1,400.00
Corruption	kg PM10	122,000.00	3,900.00	2,240.00	168,000.00
Association and bargaining rights	kg NMVOC	228,000.00	5,320.00	5,180.00	314,000.00
Biomass consumption	kg	596,000.00	16,700.00	9,060.00	2,750,000.00
Frequency of forced labor	kg 1,4-DB	593,000.00	24,100.00	13,200.00	1410,000.00
Drinking water coverage	t	-99,200.00	-4,820.00	-3,040.00	-137,000.00
Education	t CO2	39,000.00	1,340.00	1,690.00	54,900.00
Fair salary	t Fe	15,400.00	638.00	95.50	20,000.00
Industrial water depletion	kg	45,300.00	111.00	99.30	67,100.00

Goods produced by forced labor	kg CFC-11	3.11	0.10	0.08	3.75
Non-fatal accidents	kg N	-13,300.00	133.00	-2,370.00	-23,400.00
Pollution	kg P	14,300.00	638.00	287.00	33,800.00
Sanitation coverage	t 1,4-DB	691,000.00	28,100.00	236,000.00	1,590,000.00
Fatal accidents	t oil	10,100.00	285.00	357.00	13,900.00
Illiteracy	t 1,4-DB	583,000.00	28,000.00	14,700.00	2,180,000.00
Youth illiteracy	kg 1,4-DB	49,700.00	1,500.00	831.00	96,900.00
Trade unionism	kg SO2	198,000.00	5,340.00	5,270.00	355,000.00

4.1. Analysis of regional model

According to the results presented in the TO and Discussion sections, the researchers have determined the optimal sustainable impact data of the bridges by utilizing the TO process and the scientific algorithm model described in the Methodology section. The article also presents an influence curve model of sustainable development for the four bridge areas.

Establish a MATLAB scientific algorithm program to complete the regional model design:

The fitting curve Eq of XHJ1 is Z = (4.938e-54).*x.^10-(6.127e-46).*x.^9+(2.607e-38).*x.^8-(4.243e-31).*x.^7+(1.932e-24).*x.^6 - (3.69e-18).*x.^5 +(3.212e-12).*x.^4-(1.148e-06).*x.^3+0.1004.*x.^2+5371.*x-(2.681e+07); R^2 = 0.5972. (10)

The fitting Eq of SXM2 is Z = (3.034e-46).*x.^9-(1.376e-38).*x.^8 + (1.793e-31).*x.^7-(5.606e-25).*x.^6 + (7.269e-19).*x.^5- (4.506e-13).*x.^4+ (1.387e-07).*x.^3 - 0.0203.*x.^2 + 1144.*x - (1.212e+06); R^2 = 0.5408. (11)

The fitting Eq of WLT3 is Z = (3.369e-45).*x.^10 - (4.028e-38).*x.^9 + (1.51e-31).*x.^8 - (1.981e-25).*x.^7+ (8.52e-20).*x.^6-(1.367e-14).*x.^5 + (4.837e-10).*x.^4 + (5.877e-05).*x.^3 - 4.052.*x.^2 + (4.98e+04).*x - (9.724e+06); R^2 = 0.6487. (12)

The fitting Eq of JMD4 is Z = (1.804e-55).*x.^10 + (1.122e-48).*x.^9 - (2.718e-39).*x.^8 +(1.362e-31) .*x.^7-(9.779e-25).*x.^6 + (2.718e-18).*x.^5 – (3.472e-12).*x.^4+(2.008e-06).*x.^3-0.4511*x.^2+(3.578e +04).*x -(5.617e+07); R^2 = 0.4247. (13)

4.2. Analysis of regional and SA data (2008~2020)

In the face of rapid global economic growth, the country has established medium to long-term financial targets, allocating essential resources and funding to prioritize key construction projects to promote economic expansion. However, this has resulted in significant environmental degradation and adverse effects on global ecology (Chai et al., 2021). The researchers analyzed the data from the national economy and the regional government's annual social development statistical bulletin, covering the period from 2008 to 2020. These data are critical indicators of the region's economic development (Tan et al., 2017; Raimbault et al., 2020).

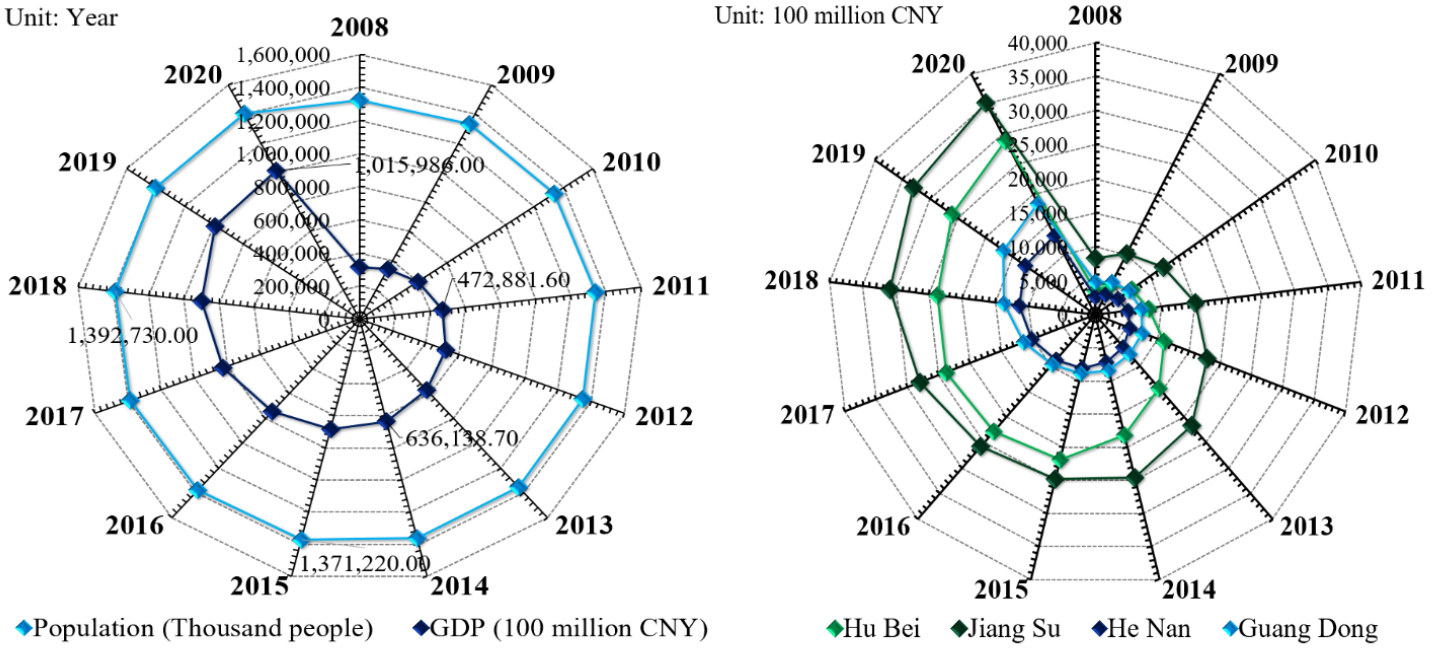

Fig. 14. Data: (a) Country data. (b) Region data (Value of construction; 2008-2020) (National Bureau of Statistics, 2021).

From 2008 to 2020, the researchers conducted a regional data analysis to evaluate the sustainable development of the construction industry in Hubei, Jiangsu, Henan, and Guangdong provinces. Utilizing Eqs (10) ~ (13) and Fig. 14, the program was applied to analyze the impact data over this period, as shown in Table 8. The results indicate that the growth rate of LCA was faster in Jiangsu and Hubei provinces, while Henan and Guangdong experienced slower growth. The SIA growth rate was faster in Jiangsu but slower in the other three regions. As of 2020, the total LCC was 725,662.282 billion CNY, LCA was 24,581,092,229.65 t, and SIA was 24,464,808,191.98 t for the four provinces.

Table 8

Regional sustainable analysis data (Unit of LCA or SIA: t).

Year		2008	2009	2010	2011	2012	2013	2014
Hu	LCA	129,763,901.56	124,683,407.88	118,950,431.03	114,404,319.26	104,611,267.47	94,367,445.33	82,701,325.44
Bei	SIA	2,380,269.04	13,305,110.33	25,877,160.23	36,036,709.14	58,518,710.43	82,954,142.28	112,002,628.23
Jiang	LCA	1,802,172,840.23	1,719,725,242.73	1,565,955,909.72	1,302,275,160.23	980,692,865.13	550,414,136.45	270,112,443.01
Su	SIA	678,984,972.52	828,791,134.88	988,941,759.96	1,179,530,700.09	1,364,226,607.24	1,574,882,885.15	1,699,287,177.26
He	LCA	2,490,819,562.92	1,827,006,963.90	1,174,425,964.73	642,887,065.41	288,867,503.38	73,373,928.72	388,521,969.80
Nan	SIA	98,348,558.39	115,483,291.00	132,684,631.20	146,274,027.45	153,185,970.72	155,425,906.09	153,291,381.57

Guang	LCA	114,331,077.32	115,637,844.31	117,031,000.54	118,279,549.55	119,194,134.13	120,233,995.17	121,278,457.96
Dong	SIA	36,454,204.55	61,317,964.73	89,376,197.74	116,144,349.43	136,916,336.95	161,971,601.26	189,019,150.94

Year		2015	2016	2017	2018	2019	2020	Total
Hu	LCA	72,210,052.72	69,263,483.69	66,776,826.48	66,770,675.71	60,621,055.23	53,099,292.69	1,158,223,484.48
Bei	SIA	139,306,931.53	147,185,978.13	153,908,922.49	153,925,636.07	170,847,003.24	192,127,473.06	1,288,376,674.20
Jiang	LCA	253,939,616.55	176,258,770.39	535,201,683.79	442,789,558.38	190,364,305.63	639,214,151.06	10,252,857,912.90
Su	SIA	1,706,275,558.22	1,739,708,984.01	1,793,177,009.72	1,820,257,606.05	1,806,203,247.56	1,762,636,720.32	18,942,904,363.00
He	LCA	657,571,895.16	804,307,455.90	922,744,126.48	899,959,221.74	748,371,797.96	677,661,766.13	11,596,519,222.23
Nan	SIA	147,379,240.14	140,203,092.33	124,005,603.83	103,625,322.84	78,877,432.41	70,591,487.67	1619,375,945.63
Guang	LCA	122,377,120.46	123,175,313.49	124,340,941.63	125,289,907.62	126,062,869.02	126,259,398.83	1,573,491,610.03
Dong	SIA	220,079,876.01	244,850,966.12	285,809,115.00	325,811,105.05	366,857,516.69	379,542,824.70	2,614,151,209.16

The results of the Andrews multivariable data matrix analysis (illustrated in Fig. 15) indicate the regional sustainable impact data trends in the four provinces from 2008 to 2020. The findings reveal that Guangdong Province has a stable and low-growing regional LCA, while Jiangsu Province has a consistently low growth rate for regional LCC and SIA. Based on this preliminary analysis, the optimal combination for evaluating sustainable development is:

$$\mathrm{LCA}_{\mathrm{Guang\ Dong}} \sim \mathrm{LCC}_{\mathrm{Jiang\ Su}} \sim \mathrm{SIA}_{\mathrm{Jiang\ Su}} \tag{14}$$

The sustainable data analysis from 2008 to 2020 used Eq (14) to establish the construction industry's impact on sustainable development. By utilizing regional LCC, LCA, and SIA data from 2008 to 2020, the researchers created a fitted equation to reflect the sustainability assessment over this period. The fitted sustainable assessment equation from 2008 to 2020 is as follows:

$$Z_{2008-2020} = -3.297e\text{-}76*x^{10}+1.83e\text{-}66*x^{9}-4.466e\text{-}57*x^{8}+6.311e\text{-}48*x^{7}-5.709e\text{-}39*x^{6}+3.451e\text{-}30*x^{5}-1.409e\text{-}21*x^{4}+3.83e\text{-}13*x^{3}-6.621e\text{-}05*x^{2}+6543*x-2.746e+11;\ R^2 = 0.9985. \tag{15}$$

$$Z_{2008-2020} = -1.705e\text{-}76*x^{10}+9.45e\text{-}67*x^{9}-2.299e\text{-}57*x^{8}+3.227e\text{-}48*x^{7}-2.889e\text{-}39*x^{6}+1.721e\text{-}30*x^{5}-6.9e\text{-}22*x^{4}+1.835e\text{-}13*x^{3}-3.097e\text{-}05*x^{2}+2994*x-1.253e+11;\ R^2 = 1. \tag{16}$$

The LCA and SIA data from 2008-2020 were analysed using Eqs (15) and (16). The interpolation algorithm was applied to the data, resulting in the following values for LCC, LCA, and SIA. From 2008 to 2020, the total emissions were LCA = 355,583,289,553.82 tons and SIA = 162,250,900,551.42 tons. The LCA emissions from the four regions accounted for 6.91% of the total emissions, SIA accounted for 15.08%, and LCC accounted for 33.95%.

The multiform approximation fitting was conducted according to the data of LCC, LCA, and SIA of four provinces from 2008 to 2020, and the sustainable impact data curve was obtained:

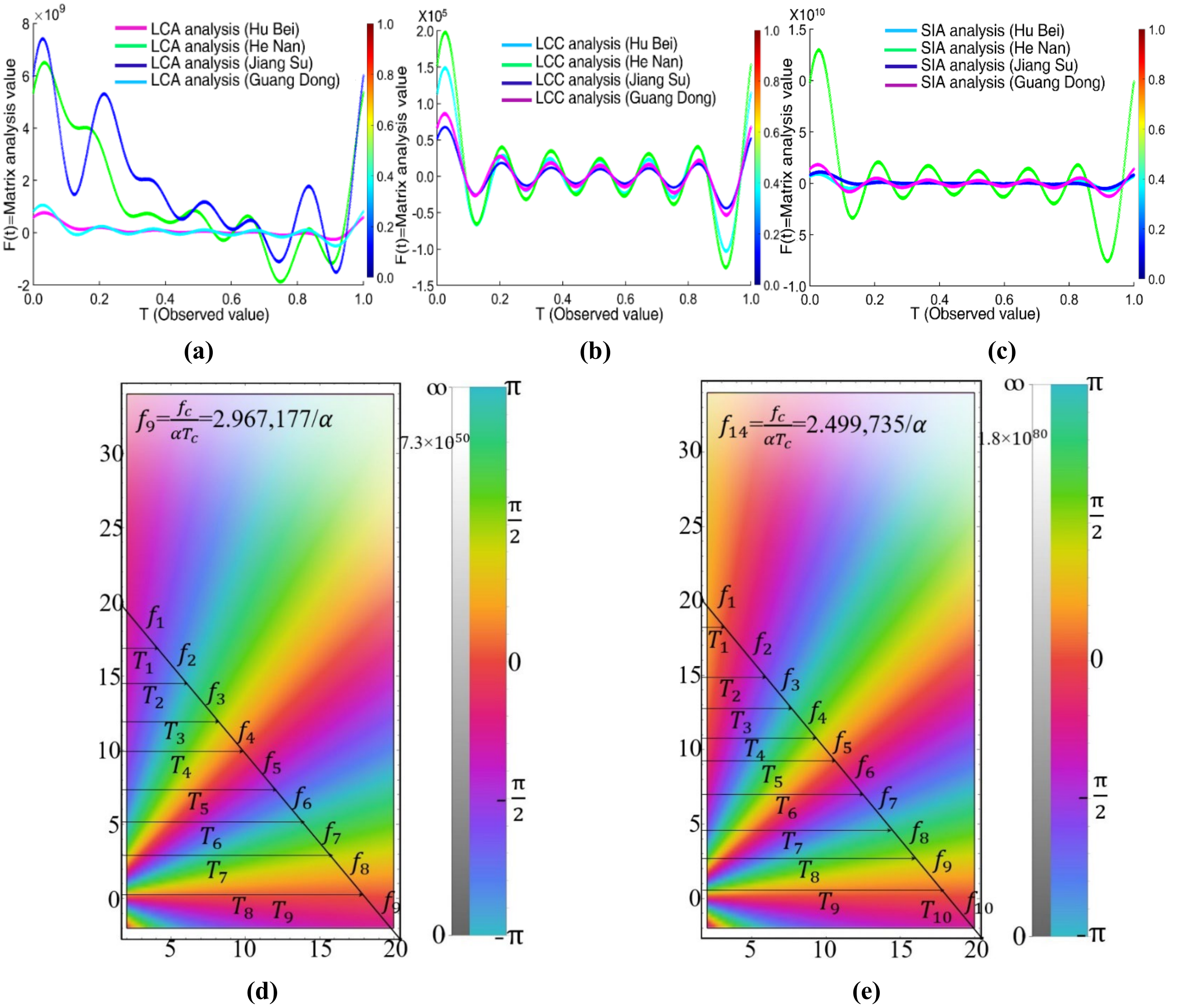

Fig. 15. Sustainable analysis of 2008–2020-year, a-f: (a) LCA. (b) LCC. (c) SIA. (d) Wavelet Transform of Eq (9). (e) Wavelet Transform of Eq (14).

Z_{Province} = (1.393e+08)+(3.69e+04).*x+0.8975.*y+0.1504.*x.^2+(-2.038e-5).*x.*y+(-4.555e-10).*y.^2+(-2.446e-06).*x.^3+ (3.061e-11). *x.^2*y + (7.133e-15). *x.*y.^2 + (4.415e-20).*y.^3; % R-square: 1. (17)

Z_{Country} = (-2.109e+12)+(7.588e+05).*x+221.6.*y-0.03248*x.^2+(-5.483e-05).*x.*y+(-7.714e-09).*y.^2+ (3.716e-10).*x.^3+ (1.178e-12).*x.^2*y+ (9.903e-16).*x.*y.^2 +(8.955e-20). *y.^3; % R -square: 1. (18)

After obtaining the optimal Eqs (15) ~ (18) and basic Eqs (10) ~ (13), this article utilizes the wavelet transform signal processing technique, a powerful tool for time-frequency analysis with a wide range of applications

(Abdulhay et al., 2020). Eqs (10) and (15) were selected and used in a Mathematica plotting program to generate Figs. 15d, e, showcasing the robustness of the research equations.

The analytical Morse wavelets of different images are obtained through parameter optimization, and the value of the symmetry parameter f_c, the time-bandwidth T_s, and the size of the image judgment frequency f ($f = f_c/T_C \times \alpha$); α is the function factor). The wavelet analysis data of Figs. 15d, e is 2.967,177/α and 2.499,734,7/α, respectively. The comparison concludes that Eq (15) is the best TO model and paradigm.

4.3. Analysis of SA data (2021~2100)

The World Bank uses the following criteria to measure a nation's economic level: 1. Low-income countries: per capita GDP less than \$875. 2. Middle-income countries: per capita GDP between \$875 and \$14,600, with an average annual GDP growth rate lower than 3.5%. 3. High-income countries: per capita GDP greater than \$14,600 (Kohli et al., 2012). The Chinese government has established the economic reform and opening (1978-2078), with a per capita GDP of USD 85,000 (Yanbin, 2021). According to research by Schrijvers et al. (Schrijvers et al., 2020), the GDP growth rate is expected to range from 3.9% to 5.3% from 2021 to 2025 and 3.1% from 2026 to 2035. Based on this research, the GDP data from 2021 to 2100 is analyzed, and the annual gross output value of the construction industry is analyzed concerning the GDP. Conclusions of this research (2021-2033): LCC, LCA, SIA (Figs. 16, 17). The data modeling and analysis were completed using a computer program compiled by Matlab. The analysis process and detailed digital programming are shown in Fig.16 and Extended Data.

Fig. 17a depicts the construction industry's output value of the Life Cycle Cost (LCC) from 2021 to 2100. In 2062, the output value of the construction industry was CNY 1.441,430,8 trillion, which represented 0.25% of the GDP in that year. After 2062, LCC enters the negative value zone, showing three mutation peaks in 2029, 2099, and 2100, respectively. From 2030 to 2062, LCC follows a quadratic parabolic curve, with a maximum peak of CNY 171.101 trillion in 2048, which accounted for 37.82% of the GDP in that year. The negative value zone appears from 2062 to 2090, with a maximum negative peak of CNY 246.915 trillion in 2079.

Fig. 17b represents the LCA impact curve. The emission values fluctuated between 27,324,944,526 to 26,279,915,920 tons between 2021 and 2045, with an average value of 26,941,413,381 tons. The LCA values showed a 10.92% variation slope from 2047 to 2059, with a maximum value of 26,696,279,176 tons. From 2060 to 2085, emissions steadily increased at a rate of 4.29%, with a low point of -4,713,252,851,939.3 t in 2079. Of particular interest was the observing of a parabolic mutation in LCA values from 2086 to 2098, with a maximum of 31,072,881,576.81 t in 2094 and an average of 15,717,785,539.26 t.

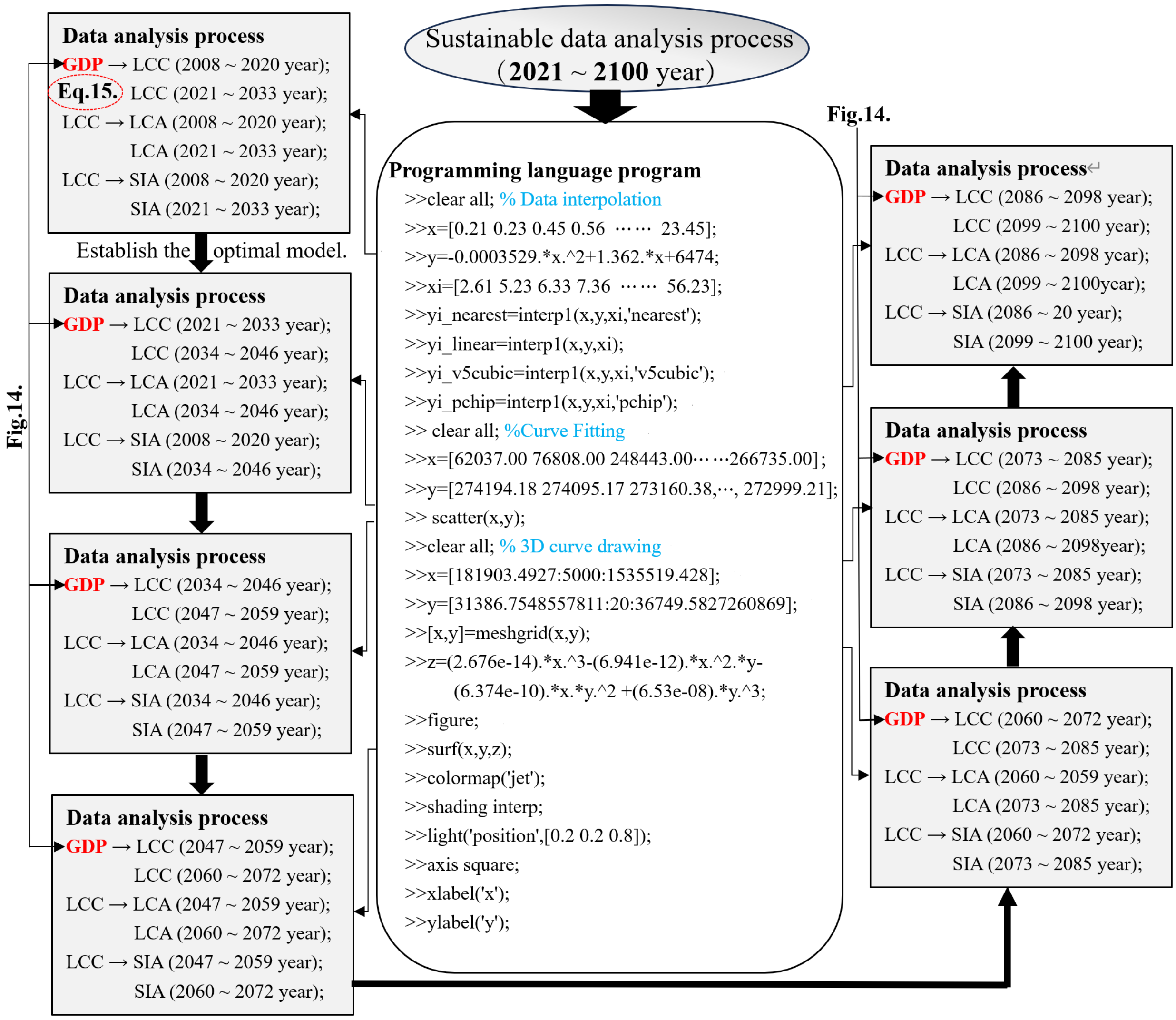

Fig. 16. Calculation and analysis program for sustainable data in the construction industry from 2021 to 2100.

According to the analysis method, the following data was obtained:

The results of SIA significantly impact sustainable development. A comprehensive policy framework addressing climate change and ecological development is crucial to tackling this global challenge (Zafar et al., 2020). Despite the importance placed on controlling and preventing LCC and LCA by researchers and government sectors, there must be more research and control measures related to SIA, which is a severe issue (Forestier and Kim, 2020). The findings of this research have raised concerns among governments worldwide. Fig. 17b shows that the SIA values show a negative trend starting in 2060, with a maximum value of 85,176,056,192t in 2079. The SIA trend is more dispersed than LCC, LCA, and GDP.

On the other hand, the period from 2021 to 2059 shows a positive change in the SIA values, reaching a maximum peak value of 42,563,178,221.27t in 2048. A mutation occurs in 2060; the SIA values remain negative until 2098, with a favourable mutation period from 2099 to 2100. The total GDP of China from 2008 to 2100 is CNY 43.540,212,703 quadrillion, as shown in Fig. 17-a, with a discreteness trend in all four variables.

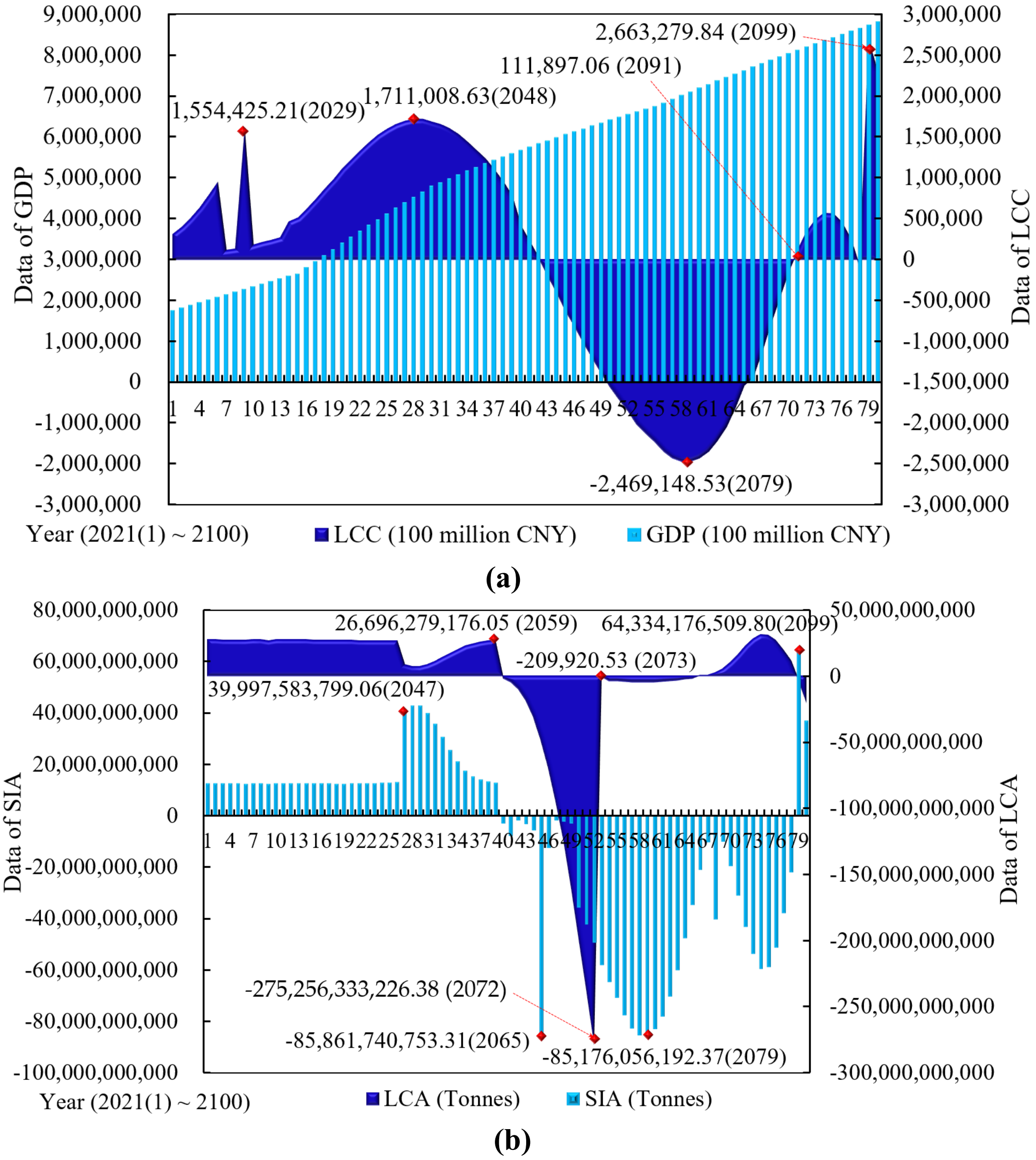

Fig. 17. Analysis of 2021–2100-years, a-b: (a) LCC and GDP. (b) LCA and SIA.

4.4. Analysis of SA data (2030~2060)

In 2019, at the 75th Session of the United Nations General Assembly, China pledged to peak its CO2 emissions by 2030 and achieve carbon neutrality by 2060 (Zafar et al., 2020). This research found that LCA emissions peaked at 27,324,944,526 t in 2030. From 2021 to 2030, LCA is in a fluctuation range, with an average change rate of 0.02%, reaching a peak in 2030. It will continue to be in the decreasing stage from 2022 to 2059, with a decreasing rate of -3.97%. In 2060, the lowest point of emissions was -1,823,196,067.86 t. It was continuously in the negative range from 2061 to 2085, with an average change rate of 51.37%. It has been in the positive range since 2086. SIA has been negative since 2060, with a continuous negative range from 2061 to 2098, with an average change rate of 79.51%. It has been positive since 2099. it has significantly contributed to global ecology and sustainability (Fig. 18).

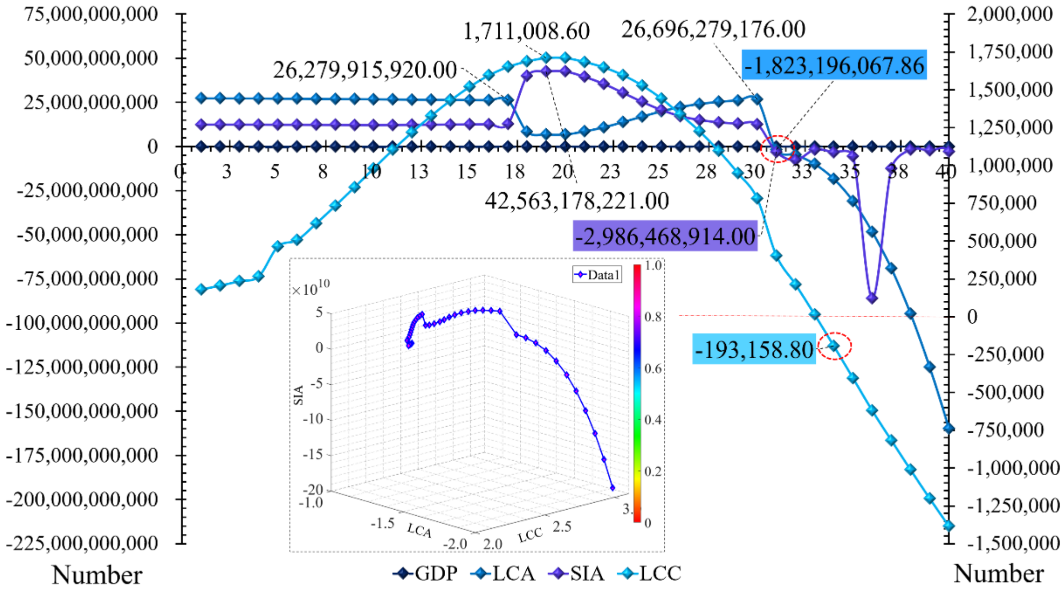

Fig. 18. Analysis of 2030、2060-years.

5. Conclusion

This research presents the optimal theoretical model for the sustainable development assessment of the regional and national construction industry by conducting optimization research on representative construction industry cases in the most developed economic regions. The research was carried out in two phases, from 2008 to 2020 and 2021 to 2100.

The findings of the case research analysis revealed that the LCA emissions of China's construction industry are expected to peak in 2030, transitioning into emissions by 2060 and staying within that range. From 2061 to 2100, the total emissions will amount to -113.55 Gt with an average annual emission of -2.77 Gt. Similarly, the SIA emissions will begin in 2060, with total emissions from 2061 to 2100 estimated at -150.02 Gt and an average annual emission of -3.75 Gt. The research data also indicates that the LCA emissions from 2008 to 2100 will total 136.451 billion t, with SIA emissions ranging from positive 772.821 billion t from 2021 to 2100 to a comprehensive negative SIA of -669.204 billion t from 2008 to 2100.

This article provides cross-century scientific data, models and methods for sustainable research on the construction industry, government, the global construction industry and the global ecological environment. The research data and theoretical model system have crucial guiding significance and practical value. This research will break the confusion about future predictions among governments, scientists and researchers around the world and guide governments to take appropriate emission reduction policy measures based on accurate data obtained from scientific analysis to ensure effective control of sustainable development while also providing a basis for the United Nations and evaluation organizations at all levels around the world provide measurement standards and reference data.

The shortcoming of this article is that the applicability of the research theoretical system to the sustainable development assessment of other industries has yet to be studied and demonstrated. The authors intend to continue their research, focusing on integrating medium and large projects in the construction industry with the environment and community. They aim to analyze the discrete impact and contribution of new green materials to the construction industry chain and research the optimization of carbon leakage in large-scale cross-regional projects.

Authorship contribution statement

Zhiwu Zhou: Conceptualization, Methodology, Software, Formal analysis, Investigation, Funding acquisition, Data curation, Writing – original draft. **Ji Zhou**: Conceptualization, Validation, Formal analysis, Resources, Writing – review & editing, Funding acquisition, Project administration. **Bo Zhang**: Formal analysis, Funding acquisition, Resources, Project administration. **Julián Alcalá**: Conceptualization, Validation, Formal analysis, Resources, Writing – review & editing, Project administration. **Víctor Yepes**: Conceptualization, Validation, Resources, Writing – review & editing, Supervision, Funding acquisition. All authors have read and agreed to the published version of the manuscript.

Acknowledgments

The authors sincerely thank the researchers and staff members for their help and thank editors and reviewers for reviewing the manuscript.

Founding information

The authors gratefully acknowledge the funding received from the following research projects: Grant PID2020-117056RB-I00 funded by MCIN/AEI/10.13039/501100011033 and by "ERDF A way of making Europe"; Project No. 2023J50418 founded by

Hunan Natural Science Foundation Project; Project No. Gui Ke AD23026260 founded by Department of Science and Technology of Guangxi Zhuang Autonomous Region; The newly launched doctoral research project, issued by Xiang Ke University [2023] No. 75.

Conflict of interest

The authors declare no conflict of interest.

References

Abdulhay, E., Alafeef, M., Hadoush, H., & Arunkumar, N. (2020). Resting state EEG-based diagnosis of Autism via elliptic area of continuous wavelet transform complex plot. Journal of Intelligent & Fuzzy Systems, 39(6), 8599–8607. https://doi.org/10.3233/JIFS-189176.

Aghimien, D. O., Aigbavboa, C. O., & Thwala, W. D. (2019). Microscoping the challenges of sustainable construction in developing countries. Journal of Engineering, Design and Technology, 17(6), 1110–1128. https://doi.org/10.1108/JEDT-01-2019-0002.

Beaudoin, S., Simard, P., & Chaloux, A. (2023). La 27e Conférence des Parties de la Convention-cadre des Nations unies sur les changements climatiques : un bilan critique. Canadian Journal of Political Science, 56(2), 474–482. https://doi.org/10.1017/S0008423923000264.

Briseghella, B., Fenu, L., Feng, Y., Lan, C., Mazzarolo, E., & Zordan, T. (2016). Optimization Indexes to Identify the Optimal Design Solution of Shell-Supported Bridges. Journal of Bridge Engineering, 21(3), 04015067. https://doi.org/10.1061/(ASCE)BE.1943-5592.0000838.

Cai, J., Wang, C., & Fu, Z. (2020). Robust concurrent topology optimization of multiscale structure under single or multiple uncertain load cases. International Journal for Numerical Methods in Engineering, 121(7), 1456–1483. https://doi.org/10.1002/nme.6275.

Carbonell, A., González-Vidosa, F., & Yepes, V. (2011). Design of reinforced concrete road vaults by heuristic optimization. Advances in Engineering Software, 42(4), 151–159. https://doi.org/10.1016/j.advengsoft.2011.01.002.

Casals, X. G. (2006). Analysis of building energy regulation and certification in Europe: Their role, limitations and differences. Energy and Buildings, 38(5), 381–392. https://doi.org/10.1016/j.enbuild.2005.05.004.

Chai, J., Hao, Y., Wu, H., & Yang, Y. (2021). Do constraints created by economic growth targets benefit sustainable development? Evidence from China. Business Strategy and the Environment, bse.2864. https://doi.org/10.1002/bse.2864.

CHAI, Q. (2022). Research on China's Pathways to Achieve Carbon Peaking and Carbon Neutrality Goals. Chinese Journal of Urban and Environmental Studies, 10(02). https://doi.org/10.1142/S2345748122500075.

China, M. of T. of the P.R. of, (2015). "General Code for Design of Highway Bridges and Culverts" (JTG D60-2015)-Traffic Books-Ministry of Transport of the People's Republic of China. Minist. Transp. People's Repub. China. https://www.mot.gov.cn/jiaotongtushu/201512/t20151229_1967723.html (accessed April 2023).

Cole, D. J., & McCrea, R. S. (2016). Parameter redundancy in discrete state-space and integrated models. Biometrical Journal. Biometrische Zeitschrift, 58(5), 1071–1090. https://doi.org/10.1002/bimj.201400239.

Cooper, D. R., Ryan, N. A., Syndergaard, K., & Zhu, Y. (2020). The potential for material circularity and independence in the U.S. steel sector. Journal of Industrial Ecology, 24(4), 748–762. https://doi.org/10.1111/jiec.12971.

Deeney, P., Nagle, A. J., Gough, F., Lemmertz, H., Delaney, E. L., McKinley, J. M., Graham, C., Leahy, P. G., Dunphy, N. P., & Mullally, G. (2021). End-of-Life alternatives for wind turbine blades: Sustainability Indices based on the UN sustainable development goals. Resources, Conservation and Recycling, 171, 105642. https://doi.org/10.1016/j.resconrec.2021.105642.

Deraemaeker, A., & Worden, K. (2018). A comparison of linear approaches to filter out environmental effects in structural health monitoring. Mechanical Systems and Signal Processing, 105, 1–15. https://doi.org/10.1016/j.ymssp.2017.11.045.

Di Cesare, A., Ponzo, F. C., & Telesca, A. (2021). Improving the earthquake resilience of isolated buildings with double concave curved surface sliders. Engineering Structures, 228, 111498. https://doi.org/10.1016/j.engstruct.2020.111498.

Du, Q., Lu, X., Li, Y., Wu, M., Bai, L., & Yu, M. (2018). Carbon Emissions in China's Construction Industry: Calculations, Factors and Regions. International Journal of Environmental Research and Public Health, 15(6), 1220. https://doi.org/10.3390/ijerph15061220.

Ebhota, W. S., & Tabakov, P. Y. (2021). Development of domestic technology for sustainable renewable energy in a zero-carbon emission-driven economy. International Journal of Environmental Science and Technology, 18(5), 1253–1268. https://doi.org/10.1007/s13762-020-02920-9.

Enright, B., Carey, C., & Caprani, C. C. (2013). Microsimulation Evaluation of Eurocode Load Model for American Long-Span Bridges. Journal of Bridge Engineering, 18(12), 1252–1260. https://doi.org/10.1061/(ASCE)BE.1943-5592.0000546.

Eze, E. C., Aghimien, D. O., Aigbavboa, C. O., & Sofolahan, O. (2022). Building information modelling adoption for construction waste reduction in the construction industry of a developing country. Engineering, Construction and Architectural Management. https://doi.org/10.1108/ECAM-03-2022-0241.

Forestier, O., & Kim, R. E. (2020). Cherry-picking the Sustainable Development Goals: Goal prioritization by national governments and implications for global governance. Sustainable Development, 28(5), 1269–1278. https://doi.org/10.1002/sd.2082.

Forman, P., Gaganelis, G., & Mark, P. (2020). Optimierungsgestützt entwerfen und bemessen. Bautechnik, 97(10), 697–707. https://doi.org/10.1002/bate.202000054.

Jiang, L., Hu, X., Zhang, G., Chen, Y., Zhong, H., & Shi, P. (2022). Carbon Emission Risk and Governance. International Journal of Disaster Risk Science, 13(2), 249–260. https://doi.org/10.1007/s13753-022-00411-8.

Goffin, K., Åhlström, P., Bianchi, M., & Richtnér, A. (2019). Perspective: State-of-the-Art: The Quality of Case Study Research in Innovation Management. Journal of Product Innovation Management, 36(5), 586–615. https://doi.org/10.1111/jpim.12492.

Hu, W., Tian, J., Li, X., & Chen, L. (2020). Wastewater treatment system optimization with an industrial symbiosis model: A case study of a Chinese eco-industrial park. Journal of Industrial Ecology, 24(6), 1338–1351. https://doi.org/10.1111/jiec.13020.

Huang, K., & Eckelman, M. J. (2022). Appending material flows to the National Energy Modeling System (NEMS) for projecting the physical economy of the United States. Journal of Industrial Ecology, 26(1), 294–308. https://doi.org/10.1111/jiec.13053.

Kennedy, C., He, W. O., & Fung, M. (2004). Role of the construction sector in the economy of a city. Canadian Journal of Civil Engineering, 31(1), 155–159. https://doi.org/10.1139/l03-089.

Kim, K. J., Yun, W. G., Cho, N., & Ha, J. (2017). Life cycle assessment based environmental impact estimation model for pre-stressed concrete beam bridge in the early design phase. Environmental Impact Assessment Review, 64, 47–56. https://doi.org/10.1016/j.eiar.2017.02.003.

Kohli, H. A., Szyf, Y. A., & Arnold, D. (2012). Construction and Analysis of a Global GDP Growth Model for 185 Countries through 2050. Global Journal of Emerging Market Economies, 4(2), 91–153. https://doi.org/10.1177/097491011200400202.

Landler, L., Ruxton, G. D., & Malkemper, E. P. (2022). The multivariate analysis of variance as a powerful approach for circular data. Movement Ecology, 10(1), 21. https://doi.org/10.1186/s40462-022-00323-8.

Li, R., Wang, Q., Liu, Y., & Yang, X. (2021). How can Germany reduce production-based and consumption-based carbon emissions? A decomposition analysis. Carbon Management, 12(4), 335–357. https://doi.org/10.1080/17583004.2021.1937322.

Liu, X., & Xin, L. (2023). Spatial and temporal evolution and greenhouse gas emissions of China's agricultural plastic greenhouses. Science of The Total Environment, 863, 160810. https://doi.org/10.1016/j.scitotenv.2022.160810.

Li, Q., Long, R., Chen, H., Chen, F., & Wang, J. (2020). Visualized analysis of global green buildings: Development, barriers and future directions. Journal of Cleaner Production, 245, 118775. https://doi.org/10.1016/j.jclepro.2019.118775.

Liu, S., & Qian, S. (2019). Evaluation of social life-cycle performance of buildings: Theoretical framework and impact assessment approach. Journal of Cleaner Production, 213, 792–807. https://doi.org/10.1016/j.jclepro.2018.12.200.

Lu, Y., Cui, P., & Li, D. (2016). Carbon emissions and policies in China's building and construction industry: Evidence from 1994 to 2012. Building and Environment, 95, 94–103. https://doi.org/10.1016/j.buildenv.2015.09.011.

Meng, L., Zhang, W., Quan, D., Shi, G., Tang, L., Hou, Y., Breitkopf, P., Zhu, J., & Gao, T. (2020). From Topology Optimization Design to Additive Manufacturing: Today's Success and Tomorrow's Roadmap. Archives of Computational Methods in

Engineering, 27(3), 805–830. https://doi.org/10.1007/s11831-019-09331-1.

Molina-Moreno, F., Martí, J. V., & Yepes, V. (2017). Carbon embodied optimization for buttressed earth-retaining walls: Implications for low-carbon conceptual designs. Journal of Cleaner Production, 164, 872–884. https://doi.org/10.1016/j.jclepro.2017.06.246.

Navarro, I. J., Yepes, V., & Martí, J. V. (2018). Social life cycle assessment of concrete bridge decks exposed to aggressive environments. Environmental Impact Assessment Review, 72, 50–63. https://doi.org/10.1016/j.eiar.2018.05.003.

National Bureau of Statistics, (2021). National Bureau of Statistics-China Statistical Yearbook Natl. Bur. Stat. http://www.stats.gov.cn/tjsj/ndsj/ (accessed October 2023).

Onat, N. C., & Kucukvar, M. (2020). Carbon footprint of construction industry: A global review and supply chain analysis. Renewable and Sustainable Energy Reviews, 124, 109783. https://doi.org/10.1016/j.rser.2020.109783.

Ozarisoy, B., & Altan, H. (2022). Bridging the energy performance gap of social housing stock in south-eastern Mediterranean Europe: Climate change and mitigation. Energy and Buildings, 258, 111687. https://doi.org/10.1016/j.enbuild.2021.111687.

Pan, D., Yu, X., & Zhou, Y. (2023). Cradle-to-grave lifecycle carbon footprint analysis and frontier decarbonization pathways of district buildings in subtropical Guangzhou, China. Journal of Cleaner Production, 416, 137921. https://doi.org/10.1016/j.jclepro.2023.137921.

Pellan, M., Louërat, M., El Beze, J., & Habert, G. (2022). A holistic perspective on the French building and construction GHG footprint. IOP Conference Series: Earth and Environmental Science, 1078(1), 012049. https://doi.org/10.1088/1755-1315/1078/1/012049.

Penadés-Plà, V., García-Segura, T., & Yepes, V. (2019). Accelerated optimization method for low-embodied energy concrete box-girder bridge design. Engineering Structures, 179, 556–565. https://doi.org/10.1016/j.engstruct.2018.11.015.

Pons, J. J., Penadés-Plà, V., Yepes, V., & Martí, J. V. (2018). Life cycle assessment of earth-retaining walls: An environmental comparison. Journal of Cleaner Production, 192, 411–420. https://doi.org/10.1016/j.jclepro.2018.04.268.

Rahmatalla, S. F., & Swan, C. C. (2004). A Q4/Q4 continuum structural topology optimization implementation. Structural and Multidisciplinary Optimization, 27(1–2), 130–135. https://doi.org/10.1007/s00158-003-0365-9.

Raimbault, J., Broere, J., Somveille, M., Serna, J. M., Strombom, E., Moore, C., Zhu, B., & Sugar, L. (2020). A spatial agent based model for simulating and optimizing networked eco-industrial systems. Resources, Conservation and Recycling, 155. https://doi.org/10.1016/J.RESCONREC.2019.104538.

Reintjes, C., & Lorenz, U. (2021). Bridging mixed integer linear programming for truss topology optimization and additive manufacturing. Optimization and Engineering, 22(2), 849–893. https://doi.org/10.1007/s11081-020-09541-8.

Ropo, M., Mustonen, H., Knuutila, M., Luoranen, M., & Kosonen, A. (2023). Considering embodied CO2 emissions and carbon compensation cost in life cycle cost optimization of carbon-neutral building energy systems. Environmental Impact Assessment Review, 101, 107100. https://doi.org/10.1016/j.eiar.2023.107100.

Rohner, J.-C., & Kjellerstrand, H. (2021). Using logic programming for theory representation and scientific inference. New Ideas in Psychology, 61, 100838. https://doi.org/10.1016/j.newideapsych.2020.100838.

Salas, J., & Yepes, V. (2018). Urban vulnerability assessment: Advances from the strategic planning outlook. Journal of Cleaner Production, 179, 544–558. https://doi.org/10.1016/j.jclepro.2018.01.088.

Shi, L., Qi, X., Yang, Z., Tao, L., Li, Y., Qiu, J., & Jiang, X. (2023). Comparative study of greenhouse gas emission calculations and the environmental impact in the life cycle assessment of buildings in China, Finland, and the United States. Journal of Building Engineering, 70, 106396. https://doi.org/10.1016/j.jobe.2023.106396.

Shobeiri, V., & Ahmadi-Nedushan, B. (2017). Bi-directional evolutionary structural optimization for strut-and-tie modelling of three-dimensional structural concrete. Engineering Optimization, 49(12), 2055–2078. https://doi.org/10.1080/0305215X.2017.1292382.

Sun, B., Xiao, R. cheng, Ruan, W. dong, & Wang, P. bo. (2020). Corrosion-induced cracking fragility of RC bridge with improved concrete carbonation and steel reinforcement corrosion models. Engineering Structures, 208. https://doi.org/10.1016/j.engstruct.2020.110313.

Swanson, K. (2023). Centering Equity and Justice in Participatory Climate Action Planning: Guidance for Urban Governance Actors. Planning Theory & Practice, 24(2), 207–223. https://doi.org/10.1080/14649357.2023.2189288.

Tan, F., Jiang, X., & Lu, Z. (2017). Some Enlightenment on Stakeholder Engagement: An Inquiry into Sustainable Development

Disparity and Its Drivers in CHINA'S Two Leading Economic Zones. Sustainable Development, 25(6), 671–685. https://doi.org/10.1002/sd.1686.

Tranter, B., Lester, L., Foxwell-Norton, K., & Palmer, M. A. (2023). In science we trust? Public trust in Intergovernmental Panel on Climate Change projections and accepting anthropogenic climate change. Public Understanding of Science, 32(6), 691–708. https://doi.org/10.1177/09636625231165405.

Venturini, T., De Pryck, K., & Ackland, R. (2023). Bridging in network organisations. The case of the Intergovernmental Panel on Climate Change (IPCC). Social Networks, 75, 137–147. https://doi.org/10.1016/j.socnet.2022.01.015.

Wang, Y., Yu, G., Hu, G., & Liu, D. (2021). Spatial Heterogeneity of Marine Environment Changes: A Case Study in Laizhou Bay and Its Adjacent Waters, China. Journal of Ocean University of China, 20(1), 111–123. https://doi.org/10.1007/s11802-021-4383-2.

Wang, Z., Yang, D. Y., Frangopol, D. M., & Jin, W. (2020). Inclusion of environmental impacts in life-cycle cost analysis of bridge structures. Sustainable and Resilient Infrastructure, 5(4), 252–267. https://doi.org/10.1080/23789689.2018.1542212.

Wiprächtiger, M., Haupt, M., Froemelt, A., Klotz, M., Beretta, C., Osterwalder, D., Burg, V., & Hellweg, S. (2023). Combining industrial ecology tools to assess potential greenhouse gas reductions of a circular economy: Method development and application to Switzerland. Journal of Industrial Ecology, 27(1), 254–271. https://doi.org/10.1111/jiec.13364.

Yanbin, L. W. and C. (2021). China's Economic Growth and High Quality Development: 2020-2035. China Economist, 16(1), 1–17. https://doi.org/10.19602/j.chinaeconomist.2021.01.01.

Yang, X., Fang, Y., Qiu, X., & Zhu, F. (2018). Gradient effect of road transportation on economic development in different geomorphic regions. Journal of Mountain Science, 15(1), 181–197. https://doi.org/10.1007/s11629-017-4498-5.

Yu, H., Peng, F., Yuan, T., Li, D., & Shi, D. (2023). The effect of low-carbon pilot policy on low-carbon technological innovation in China: Reexamining the porter hypothesis using difference-in-difference-in-differences strategy. Journal of Innovation & Knowledge, 8(3), 100392. https://doi.org/10.1016/j.jik.2023.100392.

Zafar, M. W., Shahbaz, M., Sinha, A., Sengupta, T., & Qin, Q. (2020). How renewable energy consumption contribute to environmental quality? The role of education in OECD countries. Journal of Cleaner Production, 268, 122149. https://doi.org/10.1016/j.jclepro.2020.122149.

Zamarrón-Mieza, I., Yepes, V., & Moreno-Jiménez, J. M. (2017). A systematic review of application of multi-criteria decision analysis for aging-dam management. Journal of Cleaner Production, 147, 217–230. https://doi.org/10.1016/j.jclepro.2017.01.092.

Zeug, W., Bezama, A., & Thrän, D. (2021). A framework for implementing holistic and integrated life cycle sustainability assessment of regional bioeconomy. The International Journal of Life Cycle Assessment, 26(10), 1998–2023. https://doi.org/10.1007/s11367-021-01983-1.

Zhao, B. (2023). Granting legitimacy from non‐state actor deliberation: An example of women′s groups at the United Nations Framework Convention on Climate Change. Environmental Policy and Governance. https://doi.org/10.1002/eet.2074.

Zhou, L., Wang, X., & Ye, A. (2019). Shake table test on transverse steel damper seismic system for long span cable-stayed bridges. Engineering Structures, 179, 106–119. https://doi.org/10.1016/j.engstruct.2018.10.073.

Zhou, Y., Hu, D., Wang, T., Tian, H., & Gan, L. (2023). Decoupling effect and spatial-temporal characteristics of carbon emissions from construction industry in China. Journal of Cleaner Production, 419, 138243. https://doi.org/10.1016/j.jclepro.2023.138243.

Zhou, Z., Alcalá, J., Kripka, M., & Yepes, V. (2021). Life Cycle Assessment of Bridges Using Bayesian Networks and Fuzzy Mathematics. Applied Sciences, 11(11), 4916. https://doi.org/10.3390/app11114916.

Zhou, Z. W., Alcalá, J., & Yepes, V. (2020). Bridge carbon emissions and driving factors based on a life-cycle assessment case study: Cable-stayed bridge over hun he river in liaoning, china. International Journal of Environmental Research and Public Health, 17(16). https://doi.org/10.3390/ijerph17165953.

Zhou, Z. W., Alcalá, J., & Yepes, V. (2022a). Regional sustainable development impact through sustainable bridge optimization. Structures, 41, 1061–1076. https://doi.org/10.1016/j.istruc.2022.05.047.

Zhou, Z. W., Alcalá, J., & Yepes, V. (2022b). Research on the optimized environment of large bridges based on multi-constraint coupling. Environmental Impact Assessment Review, 97, 106914. https://doi.org/10.1016/j.eiar.2022.106914.